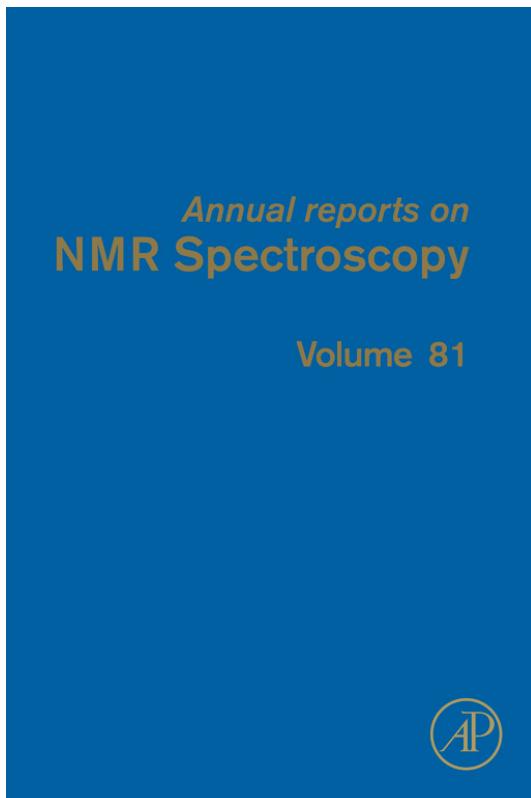


Provided for non-commercial research and educational use only.

Not for reproduction, distribution or commercial use.

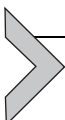
This chapter was originally published in the book *Annual Reports On NMR Spectroscopy*, Vol. 81 published by Elsevier, and the attached copy is provided by Elsevier for the author's benefit and for the benefit of the author's institution, for non-commercial research and educational use including without limitation use in instruction at your institution, sending it to specific colleagues who know you, and providing a copy to your institution's administrator.



All other uses, reproduction and distribution, including without limitation commercial reprints, selling or licensing copies or access, or posting on open internet sites, your personal or institution's website or repository, are prohibited. For exceptions, permission may be sought for such use through Elsevier's permissions site at:

<http://www.elsevier.com/locate/permissionusematerial>

From: Anmin Zheng, Feng Deng, Shang-Bin Liu, Acidity Characterization of Solid Acid Catalysts by Solid-State ^{31}P NMR of Adsorbed Phosphorus-Containing Probe Molecules. In Graham A. Webb, editor: *Annual Reports On NMR Spectroscopy*, Vol. 81, Burlington: Academic Press, 2014, pp. 47-108.
ISBN: 978-0-12-800185-1
© Copyright 2014 Elsevier Ltd.
Academic Press



CHAPTER TWO

Acidity Characterization of Solid Acid Catalysts by Solid-State ^{31}P NMR of Adsorbed Phosphorus-Containing Probe Molecules

Anmin Zheng*, Feng Deng*, Shang-Bin Liu^{†,‡}

*State Key Laboratory of Magnetic Resonance and Atomic and Molecular Physics, Wuhan Center for Magnetic Resonance, Key Laboratory of Magnetic Resonance in Biological System, Wuhan Institute of Physics and Mathematics, Chinese Academy of Sciences, Wuhan 430071, PR China

[†]Institute of Atomic and Molecular Sciences, Academia Sinica, Taipei, Taiwan

[‡]Department of Chemistry, National Taiwan Normal University, Taipei, Taiwan

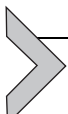
Contents

1. Introduction	48
2. Acidity Characterization by ^{31}P Solid-State NMR Spectroscopy	51
2.1 ^{31}P -TMP Approach	52
2.2 ^{31}P - R_3PO Approach	59
2.3 Other ^{31}P SSNMR Approaches Using Phosphorus-Containing Probes	63
3. Applications of ^{31}P SSNMR for Acidity Characterization	64
3.1 Discernment of Acid Types	64
3.2 Characterization of Acidic Strength	70
3.3 Location, Distribution, and Spatial Proximity of Acid Sites	94
3.4 Reaction Mechanism	100
4. Summary	103
Acknowledgements	104
References	104

Abstract

Recent developments on acidity characterization of solid acid catalysts, specifically those invoking ^{31}P solid-state nuclear magnetic resonance (SSNMR) spectroscopy using phosphorus-containing molecules as probes, have been summarized. In particular, various ^{31}P SSNMR approaches using trimethylphosphine, diphosphines, and trialkylphosphine oxides (R_3PO) will be introduced, and their practical applications for the characterization of important qualitative and quantitative features, namely, type, distribution, accessibility (location/proximity), concentration (amount), and strength of acid sites in various solid acids, will be illustrated.

Key Words: Solid acid catalysts, Phosphorus-containing molecules, Solid-state NMR, Acidity, ^{31}P chemical shift



1. INTRODUCTION

While homogeneous catalysis has been exploited for industrial petrochemical processes in the past several decades, it is handicapped by the extensive use of toxic and corrosive liquid acid catalysts such as H_2SO_4 and HF and hence also suffers from inherent high risks and costs during waste acid treatments. Thus, there has been an urgent demand in the development of heterogeneous catalysis processes, particularly those related to R&D of environmentally friendly solid acid catalysts. Over the years, a wide variety of solid acids have been developed and exploited in industrial processes, including zeolites, complex oxides, sulphated metal oxides, and heteropoly acids as depicted in [Table 2.1](#). It is well known that detailed features of acid sites, namely, their types (Brønsted vs. Lewis acid), distributions/locations (intra- vs. extracrystalline), concentrations (i.e. amounts), and strengths, normally dictate the catalytic performances (e.g. catalytic activity and product selectivity) of solid acid catalysts. Thus, a comprehensive understanding of these detailed properties of acid sites is most crucial for the design, modification, and practical applications of solid acid catalysts. For this reason, a variety of different spectroscopic and analytic techniques have been developed to unravel the nature and characteristics of acid sites in solid acids.

Common acidity characterization methods for solid acid catalysts normally utilize the direct observation of the acidic hydroxyl OH groups either by Fourier transform infrared (FTIR) [2] or ^1H nuclear magnetic resonance (NMR) [3] spectroscopy or through the analysis and/or detection of adsorbed basic probe molecules containing lone pair electrons (N, P, etc.), such as ammonia (NH_3), pyridine ($\text{C}_5\text{H}_5\text{N}$), methylamine (CH_3NH_2), or trimethylphosphine ($(\text{CH}_3)_3\text{P}$, or TMP) [4]. For the latter, analytic or spectroscopic techniques such as titration, microcalorimetry, temperature-programmed desorption (TPD), infrared (IR), and NMR are invoked [5]. In general, conventional analytic methods are more useful for quantitative description (acid amount and strength) of the *overall* acidity. On the other hand, conventional spectroscopic techniques are more suitable for qualitative characterization of acid sites. However, they are also drawback by the strong correlation between experimental parameters and surrounding environment of the solid acids. Taking HY zeolite as an example, the hydrogen-bonding

Table 2.1 List of assorted solid acid catalysts and their practical industrial applications [1]

Catalysts	Formula/example	Acid group and/or catalytic active species	Catalytic applications	Reaction type	Temperature range (°C)
Alumina (silicated)	Al_2O_3 ; $\text{Al}_{2-x}\text{Si}_x\text{O}_{3+x/2}$	AlOH , $\text{Al}-\text{OH}-\text{Al}$ $(\text{SiOH})\text{Al}^{3+}$	Olefin skeletal isomerization Alcohol dehydration	Gas/solid	>400
Silicalite	SiO_2	SiOH	Beckmann rearrangement of cyclohexanone oxime	Gas/solid	300
Chloride alumina	$\text{Al}_2\text{O}_{3-x}\text{Cl}_{2x}$	Cl_xAlOH Al^{3+}	Paraffin isomerization	Gas/solid	120–200
			Aliphatic alkylation	Liquid/solid	
Acid-treated montmorillonite clays	$\text{Na}_x[\text{Al}_{2-x}\text{Mg}_x\text{Si}^{4-}\text{O}_{10}(\text{OH})_2]\cdot n\text{H}_2\text{O}$	SiOH Al^{3+}	Cracking	Gas/solid, liquid/solid	200–550
Silica–alumina/aluminated silica	$\text{H}_y\text{Si}_{1-x}\text{Al}_x\text{O}_{2-x/2+2y}$	SiOH	Cracking, dehydrochlorination	Gas/solid	200–550
			Alkylation	Liquid/ solid	200
H-zeolites	$\text{H}_x\text{Si}_{1-x}\text{Al}_x\text{O}_2$	$\text{Si}-\text{OH}-\text{Al}$	Aromatics alkylation	Gas/solid	200–550
			Paraffin and olefin isomerization cracking	Liquid/ solid	150–250
SAPO	$\text{H}_{x-y}\text{Si}_{1-x-y}\text{P}_y\text{Al}_x\text{O}_2$	$\text{Si}-\text{OH}-\text{Al}$	Methanol to olefins	Gas/solid	400–450
Sulphated zirconia	$\text{SO}_4^{2-}/\text{ZrO}_2$	SOH	Paraffin isomerization	Gas/solid	170–230

Continued

Table 2.1 List of assorted solid acid catalysts and their practical industrial applications [1]—cont'd

Catalysts	Formula/example	Acid group and/or catalytic active species	Catalytic applications	Reaction type	Temperature range (°C)
Tungstated zirconia	WO ₃ /ZrO ₂	WOH	Paraffin isomerization	Gas/solid	200–270
Solid phosphoric acid (kieselguhr)	H ₃ PO ₄ /SiO ₂ (kieselguhr)	POH [H(H ₂ O) _n] ⁺	Olefin oligomerization and hydration Aromatics alkylation	Gas/solid	150–300
Heteropolyacid	Cs _x H _{3-x} PW ₁₂ O ₄₀	W–OH–W [H(H ₂ O) _n] ⁺	Ethyl acetate synthesis	Gas/solid	140–250
				Liquid/solid	60
Niobic acid	Nb ₂ O ₅ ·nH ₂ O	NbOH [H(H ₂ O) _n] ⁺	Ethylene hydration	Gas/solid	200
			Fructose dehydration	Water/solid	100
Sulphonated polystyrene–poly(divinylbenzene) resins	Sulphonated PPS–PDVB	–SO ₃ H [H(H ₂ O) _n] ⁺ [H(ROH)] ⁺	Ether synthesis Olefin oligomerization	Liquid/solid	40–100

interactions between the acidic proton and its adjacent framework oxygen atom are found to be much stronger in small sodalite cages than that in large supercages, leading to a considerably higher ^1H NMR chemical shift (CS; $\delta^{^1\text{H}}$) value (i.e. notable shift of ^1H resonance towards downfield) [6]. Nonetheless, this does not mean that acid sites in sodalite cages possess higher acidic strength than those in supercages. By the same token, indirect detection methods such as those through the adsorption of basic probes are also limited by the ambiguous interpretation of experimental results. For example, there have been some debates on the assignments of desorption peaks obtained from the commonly used NH_3 -TPD method [5]. The most common conception is that the multiple desorption peaks centred at low and high temperatures may be inferred to Brønsted acid sites with relatively weak and strong acidic strengths, respectively. However, *ab initio* calculations revealed that, for NH_3 adsorbed in zeolites, the dual low- and high-temperature desorption peak may be arising from interactions among encapsulated NH_3 molecules and interactions between NH_3 and the zeolite pore walls, respectively. Provided that the shape and size of the pores are similar, the finding earlier prevailed even in the absence of strong acid centres in zeolite [7]. Apparently, the notion whether NH_3 -TPD is a reliable technique for acidity characterization of solid acid catalysts remains questionable.



2. ACIDITY CHARACTERIZATION BY $^{^3\text{P}}$ SOLID-STATE NMR SPECTROSCOPY

Among various experimental methods available for acidity characterization of solid acid catalysts, solid-state nuclear magnetic resonance (SSNMR) spectroscopy is a desirable and most versatile technique. Among them, ^1H magic-angle-spinning (MAS) NMR represents a direct approach to identify structures of hydroxyl groups in a catalyst. Typically, protons residing at Brønsted acid sites, for example, bridging hydroxyls ($\text{Si}-\text{OH}-\text{Al}$) in zeolites or strongly acidic terminal hydroxyls ($-\text{OH}$) in heteropolyacids (HPAs), possess $\delta^{^1\text{H}}$ in the range of 3.6–5.6 ppm, whereas weakly acidic terminal hydroxyls (e.g. $\text{Al}-\text{OH}$ or $\text{Si}-\text{OH}$) tend to appear at 1.5–2.0 ppm [8,9]. Nonetheless, the shortcoming of this technique is its capability to explore the type, strength, and distribution of acid sites. Alternatively, MAS NMR of various adsorbed basic probe molecules, such as pyridine, acetone, and TMP, exploiting specific nucleus of interest, have been developed. For example, for the ^1H -pyridine- d_5 NMR approach, it has been found that when the pyridine- d_5 probe molecule

is adsorbed on the weakly acidic silanol groups ($\text{Si}-\text{OH}$) in zeolites, the occurrence of hydrogen-bonding interaction normally leads to resonance with $\delta^1\text{H}$ within the range of ca. 2–10 ppm. Whereas for pyridine- d_5 adsorbs on bridging hydroxyl groups ($\text{Al}-\text{OH}-\text{Si}$) in zeolites or strongly acidic terminal $-\text{OH}$ groups in HPAs, the formation of pyridinium ion ($\text{C}_5\text{D}_5\text{NH}^+$) complexes typically results in $\delta^1\text{H}$ in the range of ca. 12–20 ppm [9,10]. The ^{13}C -acetone NMR approach, which utilizes isotope-labelled 2- ^{13}C -acetone as the probe molecule, is another well-established acidity characterization technique for determining relative Brønsted acidic strengths in solid acids. Upon adsorbing the probe molecule on Brønsted acid sites, couplings between the acidic proton and the carbonyl oxygen of 2- ^{13}C -acetone normally cause the ^{13}C resonance to shift towards downfield direction (i.e. towards a higher $\delta^{13}\text{C}$ value) [11,12]. Indeed, these aforementioned ^1H -pyridine and ^{13}C -acetone NMR approaches are capable of determining the *relative* acidic strength of solid acid catalysts. However, in terms of the two key ingredients of spectroscopic techniques, namely, sensitivity and resolution, these two approaches are limited by the characteristics of their respective probing nuclei. While ^1H nucleus ($I=1/2$) has a nearly 100% natural abundance, it is handicapped by its rather narrow CS range (ca. 20 ppm), thus an inferior spectral resolution. On the other hand, although the ^{13}C nucleus ($I=1/2$) has a desirable resolution (CS range ca. 300 ppm), it has a rather low natural abundance (1.07%), thus relies on ^{13}C -enriched reagents, and hence is less favourable in terms of experimental convenience and cost.

Following the arguments mentioned earlier, phosphorus-containing molecules, such as TMP and trialkylphosphine oxides (R_3PO), should be more desirable as NMR probes. This is owing to the fact that, like ^1H and ^{13}C , ^{31}P nucleus also possesses spin $I=1/2$ but with a 100% natural abundance and a much larger CS range (>650 ppm). The main objectives of this review are twofold: (1) to provide background introduction of ^{31}P SSNMR acidity characterization technique using phosphorus-containing molecules as probes and (2) to illustrate practical applications of such technique for the characterization of acid properties (such as type, distribution, and strength) in various solid acid catalyst systems.

2.1. ^{31}P -TMP Approach

Pioneered by Lunsford and co-workers, TMP molecule was first adopted as a NMR probe to characterize the acidity of HY zeolite [13]. Thereafter, ^{31}P

MAS NMR of adsorbed TMP has been widely utilized for probing Brønsted and Lewis acidities of various solid acid catalysts, such as microporous zeolites, metal oxides, mixed metal oxides, sulphated metal oxides, and HPAs. However, as will be shown later, while the ^{31}P resonances responsible for TMP adsorbed on Lewis acid sites span over a considerable CS range of ca. –20 to –60 ppm, signals arising from TMP bound to Brønsted acid sites occur in a rather narrow range (ca. –2 to –5 ppm) [13,14]. As a consequence, the ^{31}P -TMP NMR approach is more sensitive for identifying the strength of Lewis acid sites and less sensitive for Brønsted acidity in solid acids. In this regard, as will be shown later, the ^{31}P -R₃PO NMR approach appears to be more superior in terms of identifying variations of Brønsted acid strengths in solid acid catalysts (*vide infra*).

As illustrated in Fig. 2.1, three typical interaction models may be envisaged for the adsorbed TMP with the surfaces of solid acid catalysts, namely, (i) chemisorbed on Lewis acid centres, (ii) physisorbed on weakly acidic hydroxyls (i.e. weak H-bonding interaction), and (iii) chemisorbed on Brønsted acid sites. For the latter, upon adsorbing TMP onto Brønsted acid sites, effective proton transfers from the acid site to the probe molecule result in the formation of TMPH⁺ complexes, which typically give rise to ^{31}P resonances with $\delta^{31}\text{P}$ in the range of ca. –2 to –5 ppm. Table 2.2 depicted $\delta^{31}\text{P}$ of TMP adsorbed on Brønsted and Lewis acid sites of assorted solid acids. As revealed by density functional theory (DFT) calculations, an increasing extent of proton transfer (from Brønsted acid site to TMP) would correspond to a decrease in deprotonation energy (DPE; i.e. increase in acidic strength), thus an increase in the observed $\delta^{31}\text{P}$, as shown in Fig. 2.2 [15]. In view of the fact that typical solid acid catalysts such as zeolites possess mostly Brønsted acid sites with moderate acidic strengths, corresponding to a typical DPE value of ca. 270–310 kcal/mol [15].

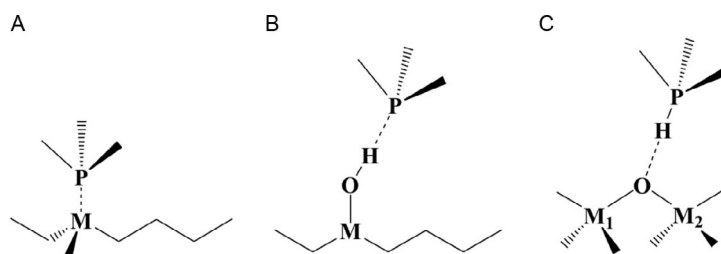


Figure 2.1 Scenarios of adsorbed trimethylphosphine (TMP) on surfaces of solid catalysts: (A) chemisorbed on Lewis acid centres, (B) physisorbed on hydroxyls, and (C) chemisorbed on Brønsted acid sites [15].

Table 2.2 Experimental ^{31}P NMR chemical shifts of TMP adsorbed on Brønsted and Lewis acid sites of various solid acid catalysts [15,16]

Catalyst	$\delta^{31}\text{P}$ (ppm)		Lewis acid centre (M)
	Brønsted acid	Lewis acid	
Al_2O_3		-51	Al
$\text{CHCl}_3/\text{Al}_2\text{O}_3$	-3.5	-44	Al
$\text{AlCl}_3/\text{Al}_2\text{O}_3$	-3.4	-41; -53	Al
H-ZSM-5	-3.5	-45	Al
H-Beta	-4.5	-32; -47	Al
HY ($T_{\text{cal}} = 700 \text{ }^\circ\text{C}$)	-4.2	-32; -43.5; -46.5; -50.5; -54.5	Al
$\text{BF}_3/\text{Al}_2\text{O}_3$	-4.0	-26	B
TiO_2		-35	Ti
$\text{SO}_4^{2-}/\text{TiO}_2$	-4.0	-24	Ti
TS zeolite	-4.8	-34.2; -32	Ti
ZrO_2		-30.3; -42.2; -50.1	Zr
$\text{SO}_4^{2-}/\text{ZrO}_2$	-3.8	-33.7; -39.7; -44.4	Zr
$\text{WO}_3/\text{ZrO}_2 (W=5.3\%)$	-4.0	-35	Zr or W
CeO_2		-19.3	Ce

Together with the well-accepted threshold DPE value for superacidity (250 kcal/mol) [18], it is noteworthy that only marginal variation in $\delta^{31}\text{P}$ was observed for the TMPH^+ adduct as DPE decreases from ca. 320 (weak acidic strength) to 250 kcal/mol (super strong acidic strength) [18]. As such, it is obvious that the ^{31}P -TMP NMR approach is inferior for differentiating Brønsted acidic strengths in solid acid catalysts.

In the case of TMP physisorbed on weakly acidic hydroxyl groups residing on the surfaces of solid acids (Fig. 2.1B), the formation of hydrogen-bonded complexes prevails, leading to ^{31}P resonance with $\delta^{31}\text{P}$ at ca. -60 ppm (Fig. 2.2). On the other hand, for TMP chemisorbed on Lewis acid sites (Fig. 2.1A), the lowest unoccupied molecular orbital of the Lewis acid centre (M) tends to share electron pairs with the phosphorus (P) atom on the TMP, and the formation of such M–P chemical bonds typically gives rise to ^{31}P signals in a considerable range of $\delta^{31}\text{P}$ within ca. -20 to -60 ppm

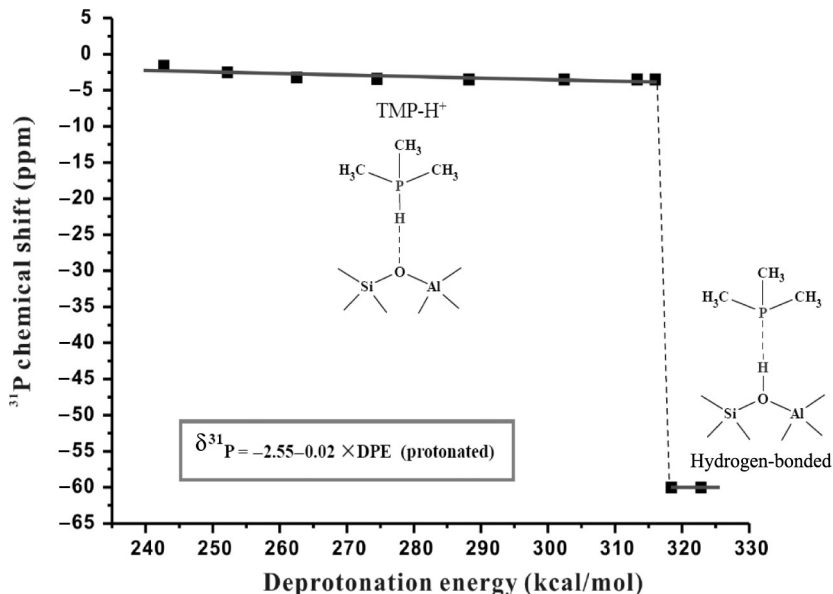


Figure 2.2 Correlations of ${}^{31}\text{P}$ chemical shift of adsorbed TMP with deprotonation energy of Brønsted acid sites in solid acids [17].

(Table 2.2). As an illustration, ${}^{31}\text{P}$ spectra obtained from mixed metal oxides by the ${}^{31}\text{P}$ -TMP NMR approach will be discussed. As shown in Fig. 2.3, three distinct ${}^{31}\text{P}$ resonances at -30.3 , -42.2 , and -50.1 ppm were observed for TMP adsorbed on zirconia (ZrO_2), indicating the presences of three types of Lewis sites with varied acidic strengths [19]. The signal responsible for TMPh^+ complex was not observed, indicating the absence of Brønsted acidic protons in the ZrO_2 catalyst. In contrast to pure ZrO_2 , a major ${}^{31}\text{P}$ peaks at -3.3 and a weak shoulder around -48 ppm were observed for TMP adsorbed on $\text{MoO}_x/\text{ZrO}_2$ (Fig. 2.3B) and WO_x/ZrO_2 (Fig. 2.3C) mixed oxide systems. The ${}^{31}\text{P}$ signal occurred at -3.3 ppm is clearly due to the presence of Brønsted acid sites, which is anticipated to exhibit much stronger acid strengths than hydroxyl groups, whereas the signal located -48 ppm was attributed to TMP adsorbed on Lewis acid sites. It is noteworthy that TMP tends to oxidize easily in these mixed metal oxides to form trimethylphosphine oxide (TMPO) during sample treatment, which attributed the ${}^{31}\text{P}$ resonance at 57.8 ppm, as can be seen in Fig. 2.3B and C [19].

The same ${}^{31}\text{P}$ -TMP NMR approach has also been employed for the characterization of sulphated metal oxides [20–22]. For TMP adsorbed on pristine TiO_2 , the symmetrical ${}^{31}\text{P}$ resonance peak centred at $\delta^{31}\text{P} \sim -35$ ppm

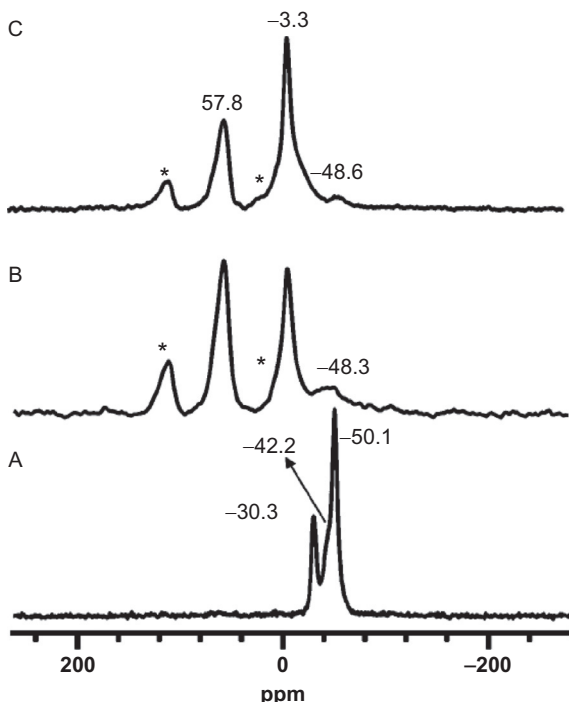


Figure 2.3 ^{31}P MAS NMR spectra (with ^1H decoupling) of TMP adsorbed on mesoporous materials: (A) ZrO_2 , (B) $\text{MoO}_x/\text{ZrO}_2$, and (C) WO_x/ZrO_2 . Asterisks denote spinning sidebands [19].

(Fig. 2.4A) may be attributed to TMP adsorbed on Lewis acid sites. Upon sulphonation treatment, a notable shift of this resonance towards downfield ($\delta^{31}\text{P} \sim -27$ ppm; Fig. 2.4B) was observed for the $\text{SO}_4^{2-}/\text{TiO}_2$ catalyst [22]. In addition, similar to that observed for $\text{MoO}_x/\text{ZrO}_2$ and WO_x/ZrO_2 in Fig. 2.3, an additional ^{31}P peak at ca. -4 ppm was also evident [19], which is unambiguously due to TMP adsorbed on Brønsted acid sites. Similar conclusions may be inferred for TMP adsorbed on pristine Al_2O_3 ($\delta^{31}\text{P} \sim -51$ ppm; Fig. 2.4C) and $\text{SO}_4^{2-}/\text{Al}_2\text{O}_3$ ($\delta^{31}\text{P} \sim -49$ and -3 ppm; Fig. 2.4D). Likewise, the additional weak peak appearing at $\delta^{31}\text{P} \sim 34$ ppm (Fig. 2.4C) has been ascribed due to the presence of TMPO. On the basis of earlier mentioned results obtained from the ^{31}P -TMP NMR approach, it is indicative while metal oxides such as ZrO_2 , TiO_2 , and Al_2O_3 possess mostly Lewis acidity, further sulphonation treatment of these metal oxide catalysts tends to not only increase the Lewis acidic strength (as indicated by the downfield shift of the ^{31}P resonance) but also promote formation of new Brønsted acid sites.

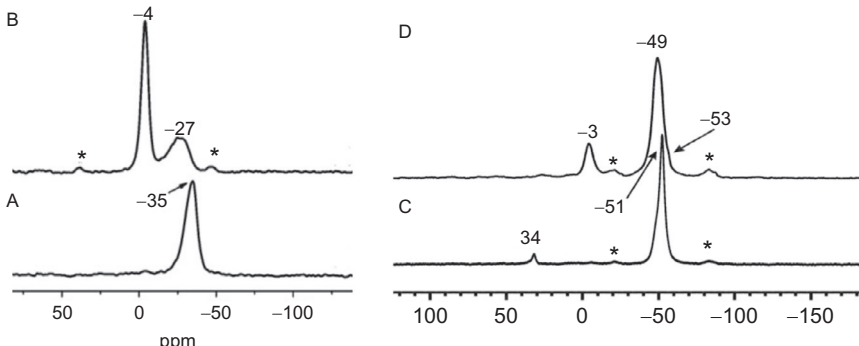


Figure 2.4 ^{31}P MAS NMR spectra of TMP adsorbed on (A) TiO_2 , (B) $\text{SO}_4^{2-}/\text{TiO}_2$, (C) Al_2O_3 , and (D) $\text{SO}_4^{2-}/\text{Al}_2\text{O}_3$. Asterisks denote spinning sidebands. The weak signal at 34 ppm in (C) is due to the presence of trimethylphosphine oxide (TMPO) [21,22].

As shown earlier, the ^{31}P -TMP approach appears to be insensitive in terms of discernment of acidic strength of Brønsted acid sites due to the limited range of $\delta^{31}\text{P}$ (-2 to -5 ppm). In this context, the same approach is more desirable for characterization of Lewis acidity, for which a much wider $\delta^{31}\text{P}$ range (ca. -20 to -55 ppm) is available. This is exemplified by a series of theoretical Lewis acid models with different metallic centres, namely, boron ($\text{BCl}_n\text{F}_{3-n}$; $n=0-3$), aluminium ($\text{AlCl}_n\text{F}_{3-n}$; $n=0-3$), and titanium ($\text{TiCl}_n\text{F}_{4-n}$; $n=0-4$). The optimized structures of assorted TMP–Lewis acid complexes are depicted in Fig. 2.5. The variations of calculated $\delta^{31}\text{P}$ with binding energy (BE) for the aforementioned theoretical Lewis acid models are shown in Fig. 2.6 [15]. Here, the BE value deduced from TMP adsorbed on the Lewis acid site is used as a criterion for evaluating the strength of Lewis acidity. It is obvious that a linear correlation between the theoretical $\delta^{31}\text{P}$ and BE may be, respectively, inferred for various Lewis acid systems with varied B, Al, and Ti centres [15]:

$$\text{BCl}_n\text{F}_{3-n} (n=0-3) : \delta^{31}\text{P} = 1.41(\pm 0.01) - 60.50(\pm 0.33) \times \text{BE}; \\ R^2 = 1.00 \quad (2.1)$$

$$\text{AlCl}_n\text{F}_{3-n} (n=0-3) : \delta^{31}\text{P} = 2.15(\pm 0.20) - 129.64(\pm 7.46) \times \text{BE}; \\ R^2 = 0.99 \quad (2.2)$$

$$\text{TiCl}_n\text{F}_{4-n} (n=0-4) : \delta^{31}\text{P} = 3.37(\pm 0.86) - 93.28(\pm 16.00) \times \text{BE}; \\ R^2 = 0.91 \quad (2.3)$$

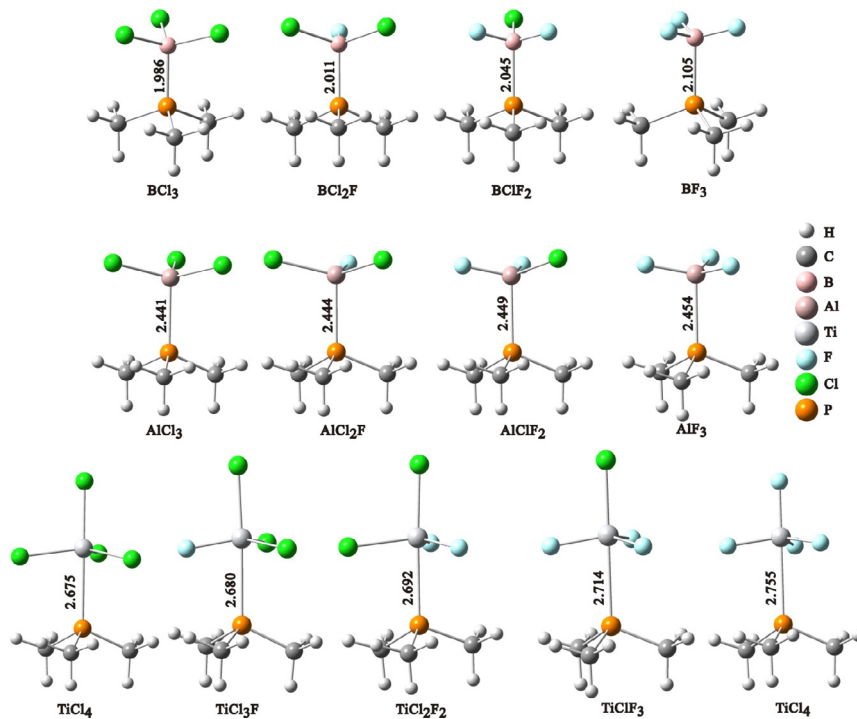


Figure 2.5 Optimized geometries of various TMP–Lewis acid complexes (see text) at the HF/6-311++G(2d,2p) level. Selective bond distances (in Å) are indicated [15].

Accordingly, such linear correlations facilitate the utilization of the ^{31}P -TMP approach for quantitative characterization of Lewis acidic strength. The $\delta^{31}\text{P}$ observed for the TMP–Lewis acid complexes indeed spans over a wider range compared to that obtained from the ^{31}P -TMPO and ^{13}C -acetone NMR approaches, indicating that the ^{31}P -TMP approach is indeed a more sensitive technique for the characterization of Lewis acidity [15]. Unfortunately, most metallic centres in a wide variety of solid Lewis acid systems tend to interact strongly with the adsorbed TMP molecule. Such complex interactions, in turn, make a universal correlation between the observed $\delta^{31}\text{P}$ and the Lewis acidic strength rather impossible for various metallic Lewis centres. This together with the fact that volatile TMP is more cumbersome to handle in terms of sample preparation represents the major shortcomings of the ^{31}P -TMP NMR approach.

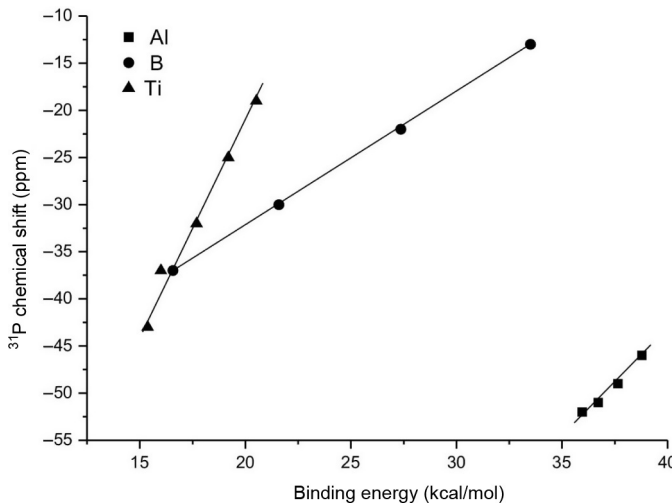


Figure 2.6 Correlations of calculated ^{31}P chemical shift with corresponding binding energy of TMP adsorbed on various Lewis acid systems with B, Al, and Ti metal centres [15].

2.2. $^{31}\text{P}-\text{R}_3\text{PO}$ Approach

As mentioned earlier, the ^{31}P -TMP NMR approach is more useful for differentiating the acid types (i.e. Brønsted and/or Lewis) and subtle differences in Lewis acidic strength in solid acids but less sensitive for Brønsted acidity. It is well known that the distribution and acidic strength of Brønsted acid sites are inhomogeneous in most solid acids; however, they normally dictate the catalytic performance of the catalysts. In this context, trialkylphosphine oxide (R_3PO ; $\text{R}=\text{C}_n\text{H}_{2n+1}$, $n=1, 2, 4, 8$) molecules, including TMPO and its homologues, namely, triethylphosphine oxide (TEPO), tributylphosphine oxide (TBPO), and trioctylphosphine oxide (TOPO), are highly desirable for probing the strength and distribution of acid sites in solid catalysts [23,24]. Comparing to the ^{31}P -TMP approach, the ^{31}P - R_3PO approach has been shown to be superior in terms of identifying variations of Brønsted acid strengths. This is due to the fact that phosphorus oxide probe molecules tend to interact with the Brønsted acid proton to form R_3POH^+ complexes, which exhibit a wide range of $\delta^{31}\text{P}$ spanning over ca. 50–98 ppm with the varied acidities. Another unique advantage of the ^{31}P - R_3PO NMR approach is that the observed $\delta^{31}\text{P}$ is directly proportional to the acidic strength of the catalyst [24].

Previously, comprehensive theoretical studies have been made to explore the correlations between the Brønsted acidic strength and $\delta^{31}\text{P}$ of adsorbed R_3PO by DFT calculations [18,25]. Accordingly, the adsorption

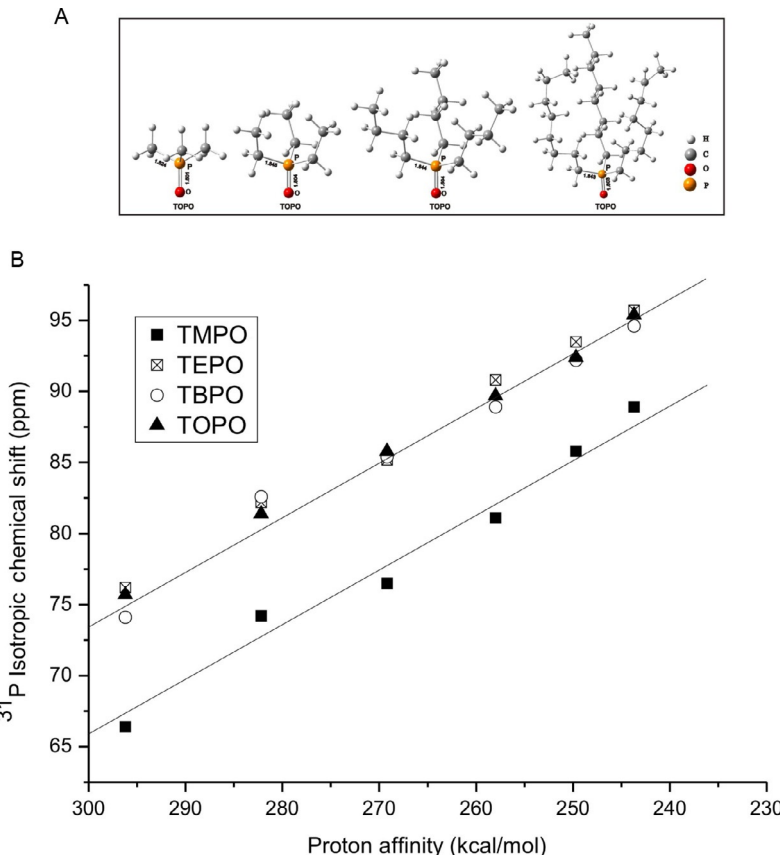


Figure 2.7 (A) Optimized equilibrium configurations of free TMPO, TEPO, TBPO, and TOPO probe molecules. Selected interatomic distances (in Å) are indicated; (B) correlations of calculated ^{31}P chemical shift of adsorbed R_3POH^+ complexes and proton affinity (PA) predicted based on the 8T zeolite cluster models [25]. Reproduced with permission from ACS.

structures and $\delta^{31}\text{P}$ of R_3PO adsorbed on Brønsted acid protons with varied acid strengths (from weak, medium, strong, to super acid) were carried out on an 8T zeolite cluster model by varying the Si–H bond distance (Fig. 2.7A). Interestingly, linear correlations between the $\delta^{31}\text{P}$ of homologous R_3PO probe molecules and the proton affinity (PA; in kcal/mol) were obtained, as shown in Fig. 2.7B. The PA value is equivalent to the DPE, that is, the energy required to rip off the proton from a Brønsted acid site. Taking TMPO as an example, the correlation can be expressed as

$$\text{TMPO : } \delta^{31}\text{P} = 182.866(\pm 5.314) - 0.3902(\pm 0.020) \times \text{PA}; \\ R_2 = 0.9913. \quad (2.4)$$

It is obvious that the linear dependences observed for TEPO, TBPO, and TOPO not only nearly overlap with one another but also exhibit a similar slope compared to that observed for TMPO (Eq. 2.4). Thus, with the exception of TMPO, variations in alkyl chain length of the R_3PO ($\text{R} = \text{C}_n\text{H}_{2n+1}$, $n = 1, 2, 4, 8$) probe molecules appear to have negligible effect on the $\delta^{31}\text{P}$ (within an experimental error of ca. ± 2 ppm) observed for corresponding R_3POH^+ adsorption complexes. Note that an average offset of 8 ± 2 ppm was observed for $\delta^{31}\text{P}$ of adsorbed $(\text{C}_n\text{H}_{2n+1})_3\text{PO}$ with $n \geq 2$ (i.e., TEPO, TBPO, and TOPO) relative to TMPO ($n=1$). On the bases of theoretical predictions and experimental results obtained from the ^{31}P -TMPO NMR approach, a threshold $\delta^{31}\text{P}$ value of ca. 86 ppm was derived for superacidity, corresponding to a threshold PA value of ca. 250 kcal/mol [18]. Consequently, a threshold $\delta^{31}\text{P}$ value of ca. 92–94 ppm may be inferred for R_3PO probes with $n \geq 2$ [25]. As such, quantitative information on acidic strength of Brønsted acid sites in solid acids may readily be attained by combining the results obtained from the ^{31}P - R_3PO NMR approach. Moreover, by incorporating spectral deconvolution with elemental analysis, quantitative information such as distribution and concentration of acid sites may also be determined [24,26].

As illustrated in Fig. 2.8, a standard operation procedure invoking the ^{31}P - R_3PO NMR experimental approach, including adsorption of guest molecules (such as TMPO or TBPO) on solid catalysts and relevant experimental considerations, has been explored [27,28]. Taking the adsorption of TMPO on typical 10-membered ring (10-MR; typical pore diameter ca. 0.6 nm) H-ZSM-5 zeolite as an example, the solid catalyst was first subjected

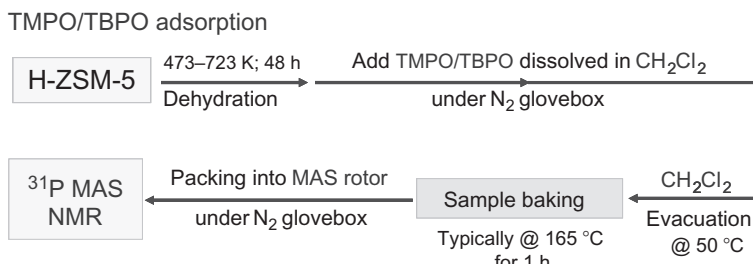


Figure 2.8 Standard operation procedure invoked for the ^{31}P - R_3PO NMR approach [27,28].

to a thorough dehydration treatment under desirable temperature and duration (for zeolites, typically 673–723 K for at least 12 h) in a vacuum manifold ($<10^{-5}$ torr) prior to the adsorption of guest molecule [16]. Subsequently, a known amount of crystalline TMPO adsorbate dissolved in anhydrous CH_2Cl_2 was introduced into a vessel containing the dehydrated solid sample under inert environment (e.g. in a N_2 bag or glove box), followed by the removal of the CH_2Cl_2 solvent by evacuation at ca. 323–343 K. To ensure a uniform adsorption of adsorbate probe molecules in the pores/channels of the porous adsorbents, the sealed sample vessel was further subjected to thermal treatment at ca. 438 K (note that the melting point of TMPO is ca. 413 K) for at least 1 h. It is noteworthy that an excessive loading of adsorbate molecules is desirable in ensuring a complete coverage of all acid sites and that adequate thermal pretreatment of the adsorbate-loaded sample is an inevitable procedure to warrant a homogeneous distribution of probe molecule on acid sites. Finally, the TMPO-loaded sample (in sealed vessel) was transferred into a MAS rotor, which is sealed by a gas-tight (Kel-F) cap, under inert environment (e.g. N_2 bag/glove box). Regarding to the subsequent solid-state ^{31}P MAS NMR experiment, typically ca. 800–1000 free-induction-decay signals were accumulated using a single pulse sequence with a recycle delay of ca. 10 s and a sample spinning frequency of ca. 12 kHz. The earlier mentioned experimental parameters are of course depending on the estimated numbers of Brønsted acid sites (or Al content in zeolite) present in the intra- and/or extracrystalline surfaces of the detecting solid catalyst.

As shown in Fig. 2.9, an extensive investigation has been made invoking the ^{31}P -TMPO approach for acidity characterization of various solid acids, including microporous zeolites (H-ZSM-5, H-mordenite, H-Beta, H-USY, and MCM-22), mesoporous molecular sieves (MCM-41), and metal oxides such as sulphated ZrO_2 [29]. Except for the latter, porous catalyst samples with a similar Al content ($\text{Si}/\text{Al} \sim 15$) were chosen for comparison purpose. It is indicative that the ^{31}P resonances and corresponding observed $\delta^{31}\text{P}$ readily render comparison of relative acid strengths in various solid catalysts. In addition, other qualitative information such as relative distribution and concentration of acid sites may be derived from the peak areas of the deconvoluted spectra. Furthermore, by combining the spectral analysis data with results obtained from elemental analysis (i.e. by ICP-MS method), quantitative information of acid sites in solid acids may also be attained, affording detailed understanding of acid features, namely, type, distribution, amount, and strength of acid sites [29].

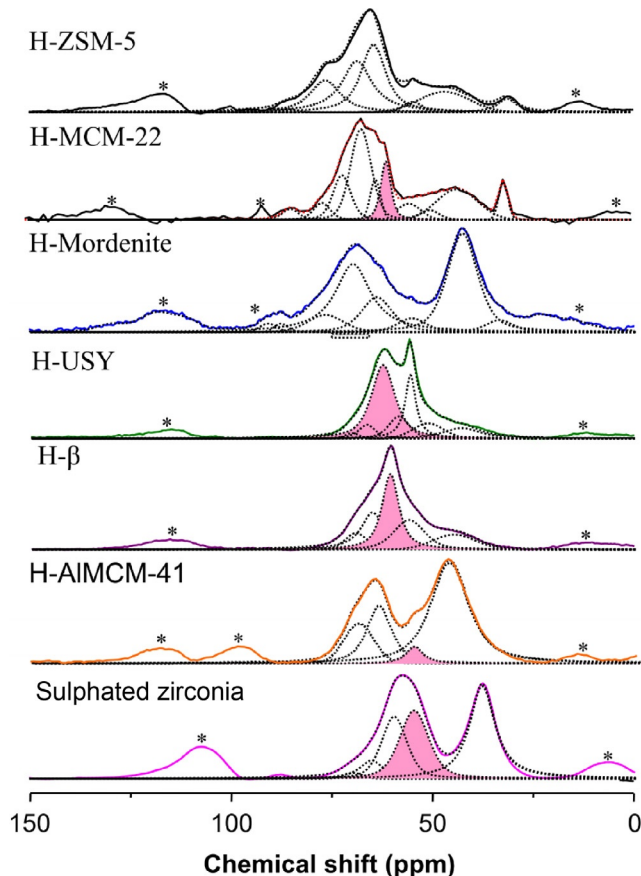


Figure 2.9 ^{31}P MAS spectrum of the TMPO loaded on various solid acid catalysts. Except for sulphated zirconia, all porous substrates have a Si/Al of ca. 15. The dashed curves are results obtained from spectral analysis by Gaussian deconvolution and the shaded peaks represent presence of Lewis acidity [29].

2.3. Other ^{31}P SSNMR Approaches Using Phosphorus-Containing Probes

In addition to the aforementioned ^{31}P -TMP and R_3PO NMR approaches, some other phosphorus-containing probe molecules have been exploited for acidity characterization in solid acid catalysts. For example, triphenylphosphine (PPh_3) molecule has been used for probing the distribution of Brønsted acid sites in solid acids [30]. Owing to its size (ca. 1.17×0.71 nm), the bulky PPh_3 molecule is desirable for detecting acid sites presiding on the external

surfaces of zeolic catalysts with 8- and 10-MR pore channels. Related applications of the ^{31}P - PPh_3 NMR approach will be illustrated in a later section. Apart from the properties of isolated acid sites, proximities of acid centres also play a crucial role during catalytic reactions that involve multiple acid sites. In this context, the homologous series of diphenyldiphosphines ($\text{Ph}_2\text{P}(\text{CH}_2)_n\text{PPh}_2$; $n = \text{integer}$) whose physical size may be tuned by varying the $-\text{CH}_2$ group in the axial position can be used to determine proximities of Brønsted acid centers in solid acid catalysts. For example, a P–P distance of 0.30, 0.56, and 0.94 nm was found for $\text{Ph}_2\text{P}(\text{CH}_2)_n\text{PPh}_2$ with $n = 1, 3$, and 6, respectively. Accordingly, Grey and co-workers utilized ^{31}P - ^{31}P DQ NMR [31] of adsorbed diphenyldiphosphine ($\text{Ph}_2\text{P}-\text{CH}_2-\text{PPh}_2$) to determine distance between adjacent Brønsted acid sites in solid catalysts [32]. The applicability of the earlier mentioned technique is, of course, relying on the fix distance between two phosphorus atoms in the probe molecule. The earlier mentioned notion was further justified by the 2D DQ-SQ (double quantum–single quantum) correlation NMR technique [31], which is capable of probing the spatial proximity of two like spins. Accordingly, by comparing the ^{31}P NMR spectra obtained from different diphenyldiphosphine probe molecules with varied P–P distances and loadings, the distance and concentration of acidic sites in zeolic catalysts may readily be determined (*vide infra*) [32].



3. APPLICATIONS OF ^{31}P SSNMR FOR ACIDITY CHARACTERIZATION

3.1. Discernment of Acid Types

As mentioned earlier, while the ^{31}P -TMP NMR approach is more useful for differentiating acidic strength of Lewis acid sites, the ^{31}P - R_3PO NMR approach is desirable for probing Brønsted acidity. In other words, in terms of validity of probe molecule, TMP is less sensitive for probing Brønsted acid sites, while R_3PO molecules are inferior for detecting Lewis acidity. Since volatile TMP is more cumbersome to handle in terms of sample preparation, the ^{31}P - R_3PO approach is more preferable in this context. Among them, TMPO represents the most popular probe molecule chosen owing to its suitable dimension (*vide supra*). In practice, differentiation of Brønsted versus Lewis acidity invoking the ^{31}P -TMPO NMR approach is normally carried out by comparing results obtained from experiments performed on fully dehydrated as well as partially hydrated samples [26]. It is known that Lewis acid sites (extraframe Al species in zeolites), which interact weakly with

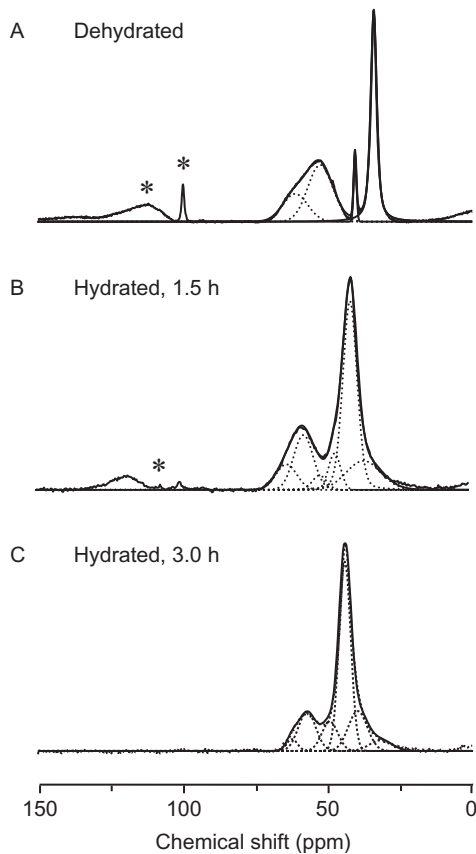


Figure 2.10 ^{31}P MAS NMR spectra of TMPO adsorbed on (A) fully dehydrated, and (B) and (C) partially hydrated ZrO_2 . The dashed curves represent spectral simulation results and the asterisks denote spinning sidebands (spinning rate 12 kHz) [26].

TMPO, may easily react with H_2O to form weak Brønsted acid sites. However, the strong bonding between TMPO and the Brønsted acid sites is unlikely to be dissociated while in the presence of H_2O . Thus, upon progressive exposure of the TMPO-loaded samples to humidity, ^{31}P resonances associated with Lewis acid sites will be diminished eventually, while those bound to Brønsted acid sites will remain intact. As such, this offers an indirect method to identify the presence of Brønsted and/or Lewis acidity in the solid catalyst. For example, Fig. 2.10 shows the ^{31}P MAS NMR spectra of TMPO adsorbed on dehydrated ZrO_2 catalyst before (Fig. 2.10A) and after partial hydration treatments (Fig. 2.10B and C). [26] Four distinct resonances at 62, 53, 41, and 34 ppm were observed for fully dehydrated pure

ZrO₂. While the latter two peaks with $\delta^{31}\text{P}$ lower than 50 ppm are unambiguously due to physisorbed TMPO, the other two peaks at 62 and 53 ppm may be, *a priori*, assigned due to TMPO adsorbed on Brønsted and/or Lewis acid sites. Upon progressive exposure of the TMPO-loaded ZrO₂ sample to humidity, the peak intensities at 62 and 53 ppm decrease with increasing severity of hydration (i.e. H₂O content), while the peaks responsible for physisorbed TMPO (at 41 and 34 ppm) are broadened and shifted towards downfield (i.e. higher $\delta^{31}\text{P}$) direction. Accordingly, the two peaks at 62 and 53 ppm observed for the parent ZrO₂ sample can thus be ascribed due to the interaction of TMPO with Lewis sites with different acidic strengths, in excellent agreement with earlier reports by IR spectroscopy of adsorbed CO [33–35].

Aside from the more sophisticated ³¹P SSNMR approaches available for indirect detection of acid types in solid acid catalysts (*vide supra*), direct identification of Brønsted and Lewis acid sites would be highly desirable. In this regard, Huang *et al.* developed a novel SSNMR technique [36] for direct discernment of Brønsted and Lewis acid sites in solid acids through simple spectral editing. This is accomplished by incorporating a selective ¹H excitation pulse on nonacidic protons while observing the ³¹P resonance in conjunction with the Lee–Goldburg cross polarization (LG-CP) method [37,38], which effectively suppress homonuclear dipole–dipole couplings. As shown in Fig. 2.11A, five distinct ³¹P resonances at 41, 45, 55, 65, and 75 ppm were observed for TMPO loaded on HY zeolite. Based on the results obtained from additional experiments using the ¹H/³¹P/²⁷Al TRAPDOR technique [39], the authors were able to assign most of the ³¹P resonance signals in Fig. 2.11A. Peaks V (75 ppm) and I (41 ppm) are ascribed due to TMPO adsorbed on strong Brønsted acid sites and physisorbed TMPO, respectively [40]. However, the assignment of peaks II (45 ppm), III (55 ppm), and IV (65 ppm) remained ambiguous. In the selective LG-CP experiment, a Gaussian-shaped pulse was used to selectively suppress the ¹H signal at 2.1 ppm (i.e. the anticipated $\delta^1\text{H}$ for nonacidic Si–OH groups in the HY zeolite) while keeping the ¹H resonance at 7.2 ppm (arising from Brønsted acid sites) unperturbed. Accordingly, the ${}^{31}\text{P}\{{}^1\text{H}\}$ selective LG-CP spectrum can thus be compared with the spectrum obtained from conventional LG-CP sequence in the absence of ¹H selective excitation to render further assignment of the ³¹P resonances, as shown in Fig. 2.11B. Note that since the spectrum obtained from selective LG-CP exhibited much weaker signal sensitivity compared to that of regular LG-CP, it was scaled up

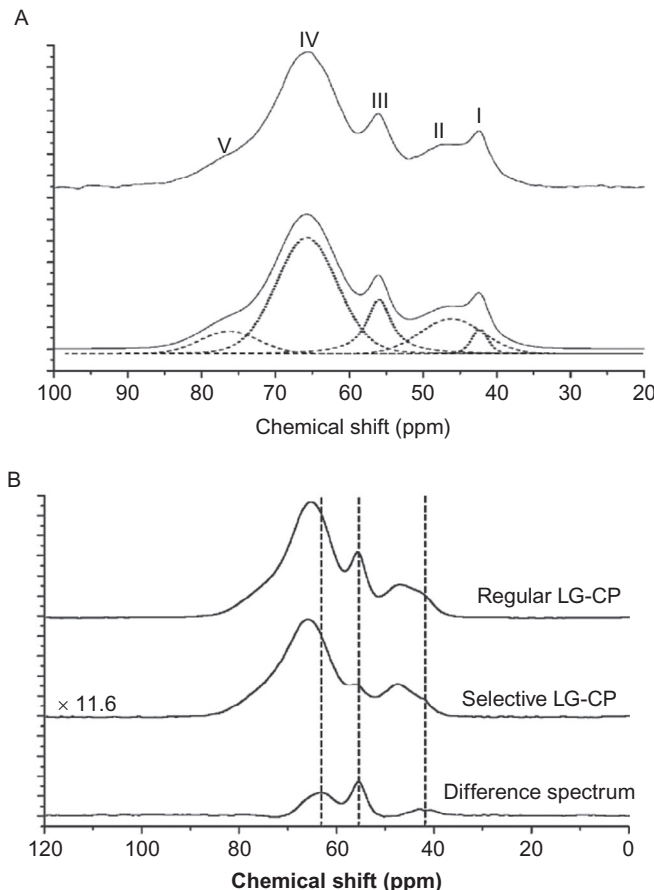


Figure 2.11 (A) Top: ^{31}P MAS NMR spectrum of TMPO adsorbed on HY zeolite ($\text{Si}/\text{Al}=2.6$). Bottom: Deconvoluted spectrum via Gaussian simulations. (B) $^{31}\text{P}\{^1\text{H}\}$ LG-CP spectra with and without selective excitation of bridging hydroxyl protons [36].

intentionally so that the most intense signal at 75 ppm (peak V) may be diminished in the difference spectrum. As a result, three ^{31}P resonance peaks at 65, 55, and 41 ppm were observed in the difference spectrum (Fig. 2.11B). *A priori*, it is anticipated that only ^{31}P signals arising from TMPO adsorbed on Lewis acid sites, silanol sites, or Brønsted acid sites that have different polarization transfer dynamics would remain in the difference spectrum. That the signal at 45 ppm is absent in the difference spectrum indicates that peak II (see Fig. 2.11A) should be solely due to TMPO adsorbed on Brønsted acid sites (with somewhat weak acidic strength), whereas the broader peak centred at ca. 41 ppm is attributed

to TMPO interacting with silanol groups. Thus, it is indicative that peaks III and IV, which are also present in the difference spectrum, should be associated with Lewis acidity. In view of their difference in peak intensity, the authors concluded that the peak at 55 ppm should be mainly due to TMPO interacting with Lewis acid sites but partially with Brønsted acidity and vice versa for the peak at 65 ppm. Nonetheless, this does not exclude the scenarios of TMPO interacting with Brønsted acid sites residing in the sodalite cages (which are inaccessible to probe molecules) of HY zeolite, forming weak hydrogen bonding through the narrow windows.

Adopting the similar spectral editing scheme, Massiot *et al.* demonstrated that chemical environments of molecular adsorbate on surfaces of mixed metal oxide catalysts may also be attained by means of ^{31}P -TMPO NMR approach [41]. As shown in Fig. 2.12(a1), when TMPO is adsorbed on precipitated silica–alumina (Al_2O_3 content 5 wt%), two main signals with $\delta^1\text{H}$ of ca. 1.5 and 7.0 ppm were observed, which may be assigned due to methyl protons on TMPO and Brønsted acid protons ($\text{Si}–\text{OH}–\text{Al}$) bound to TMPO, respectively. On the other hand, the corresponding $^{31}\text{P}\{^1\text{H}\}$ CP MAS NMR spectrum exhibited four main features, which may be attributed to crystalline TMPO (42 ppm), physisorbed TMPO (41 ppm), and TMPO adsorbed on Brønsted (site 1, 64 ppm) and Lewis (site 2, 58 ppm) acid sites [42]. It is noteworthy that the peak intensity of the ^{31}P resonance may be manipulated by varying the contact times τ_c during $^{31}\text{P}\{^1\text{H}\}$ CP or Lee–Goldburg CP (CPLG) experiments, as illustrated in Fig. 2.12(b1) and (b2), respectively. In other words, the ^{31}P resonance signals will be predominately arising from crystalline TMPO at short contact times ($\tau_c \leq 1$ ms), while the signal of TMPOH^+ arising from TMPO adsorbed on Brønsted acid sites (site 1) prevails at longer τ_c . Additional experiments by a modified 2D ^1H - ^{31}P heteronuclear correlation (HETCOR) technique, which exploits ^1H phase-modulated Lee–Goldburg homonuclear decoupling in conjunction with CPLG heteronuclear decoupling prior to the detection period, were also performed under varied contact time (τ_c) and mixing time (τ_m). Again, at short τ_c (0.5 ms) and null τ_m , a single correlation peak corresponding to ^{31}P signal of the crystalline TMPO (referred as B in Fig. 2.12(c1)) and ^1H signal of its methyl protons was observed. Upon increasing τ_c to ca. 12 ms, additional correlation peaks associated with TMPO interacting with acid sites (referred as A), ^{31}P signals, and methyl ^1H signals were evident (Fig. 2.12(c2)). A slight shift in $\delta^1\text{H}$ (ca. 0.5 ppm) was also observed between methyl ^1H signals associated with phase-separated (crystalline) and bounded TMPO. Moreover, when

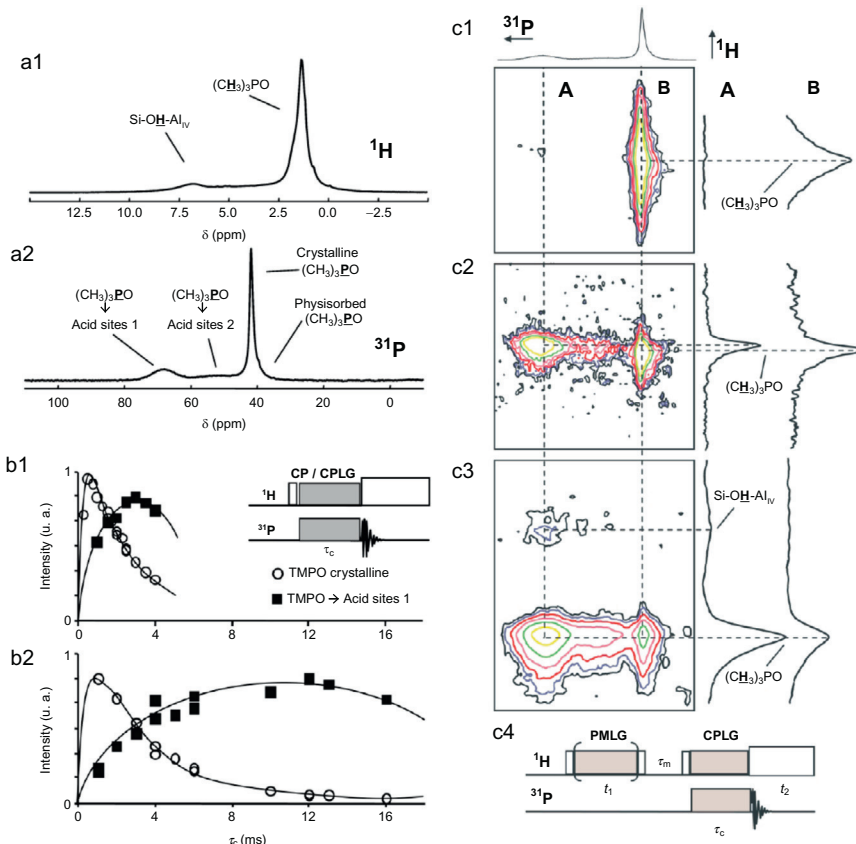


Figure 2.12 (a1, a2): (a1) ^1H MAS and (a2) ^{31}P [^1H] CP MAS NMR spectra of TMPO-loaded silica–alumina sample. (b1, b2): Variations of ^{31}P signal intensities with contact time τ_c for crystalline TMPO (○) and for TMPO in interaction with acid sites 1 (■) using (b1) CP and (b2) CP-LG pulse sequences. Lines are purely indicative. (c1–c4): 2D contour plots obtained from the ^1H - ^{31}P HETCOR experiments using the pulse sequence depicted in (c4) with (c1) $\tau_c=0.5$ ms, $\tau_m=0$ ms, 384 scans; (c2) $\tau_c=12$ ms, $\tau_m=0$ ms, 384 scans; and (c3) $\tau_c=12$ ms, $\tau_m=50$ ms, 2048 scans. Vertical ^1H spectra correspond to TMPO interacting with (A) acid sites 1, and (B) crystalline TMPO, which were obtained from a multistep fitting procedure of all rows (F1 dimension) using the four ^{31}P signals [41].

allowing ^1H spin diffusion to take place during the mixing period ($\tau_m=50$ ms; Fig. 2.12(c3)), a new correlation peak arising from ^{31}P resonance of TMPO (68 ppm) and bridging hydroxyl protons (Si–OH–Al; at ca. 7 ppm) was also observed. Accordingly, various adsorption states and interactions of the TMPO probe molecule and acid sites may be readily resolved using multinuclear NMR techniques [41].

3.2. Characterization of Acidic Strength

Apart from discernment of acid type, qualitative and quantitative measures of acidic strengths in solid acids are also crucial for the detailed understanding of the mechanism and performance of the catalyst during catalytic reactions. Assorted illustrations for characterization of acidic strength in various solid acid catalysts invoking the aforementioned ^{31}P SSNMR approaches will be discussed in this section.

3.2.1 Microporous Zeolites and Mesoporous Molecular Sieves

It has been shown that the ^{31}P SSNMR of adsorbed TMP and/or TMPO probe molecules is a practical approach for acidity characterization of solid acid catalysts. In particular, important acid features such as distribution and strength of acid sites may be readily attained. Figure 2.13 shows the ^{31}P MAS NMR spectra of TMP adsorbed in H-form mordenite (MOR; Si/Al = 10) and beta (Si/Al = 12.5) zeolites, which both possess 12-MR pores [44]. In the presence of ^1H decoupling, the ^{31}P resonance of the adsorbed TMP revealed a singlet at -2.2 (Fig. 2.13A) and -5.0 (Fig. 2.13C) ppm for H-MOR

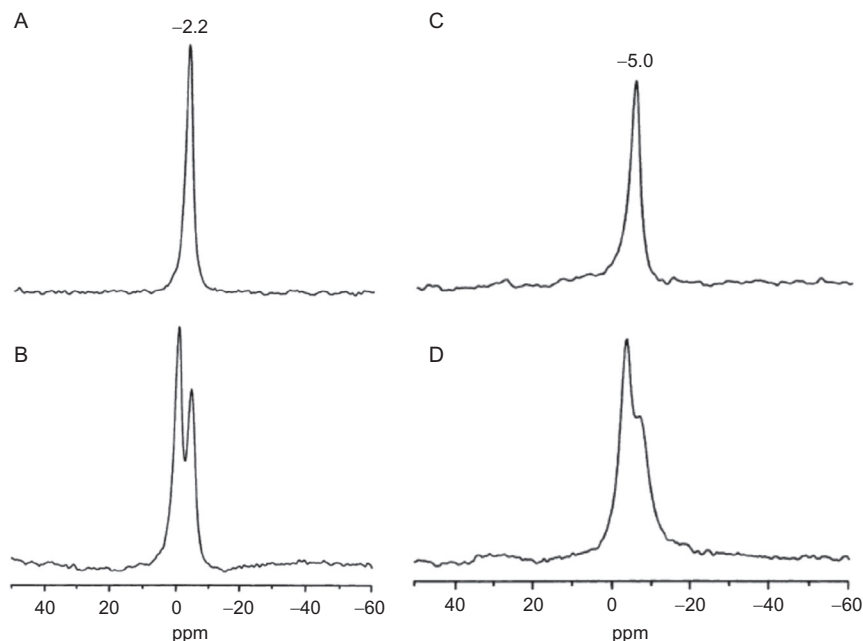


Figure 2.13 Room-temperature ^{31}P MAS NMR spectra of TMP adsorbed on H-MOR and H-beta acquired (A, C) with and (B, D) without proton decoupling (spinning frequency = 10 kHz) [43].

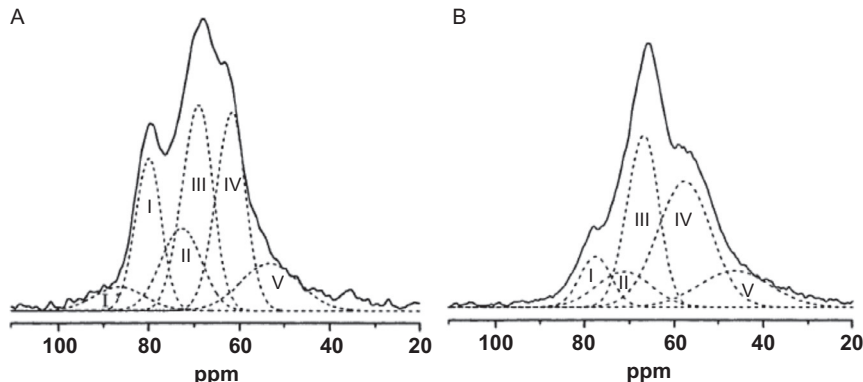


Figure 2.14 Proton-decoupled ^{31}P MAS NMR spectra of TMPO adsorbed on (A) H-MOR and (B) H-beta zeolites. Both spectra were recorded at room temperature with a spinning frequency of 10 kHz. The dashed curves represent spectral simulation results via Gaussian deconvolution.

and H-beta, respectively, revealing interaction of the probe molecule with Brønsted acid sites, forming the protonated $[(\text{CH}_3)_3\text{PH}]^+$ adduct. No ^{31}P resonance signal was observed within the $\delta^{31}\text{P}$ range of -30 to -60 ppm, indicating the absence of Lewis acidity in both zeolite catalysts. For spectra recorded without ^1H decoupling, ^{31}P resonance responsible for the $[(\text{CH}_3)_3\text{PH}]^+$ adduct splits into a well-resolved doublet, as shown in Fig. 2.13B and D. Accordingly, a corresponding J -coupling constant ($J_{\text{P}-\text{H}}$) of 493 and 409 Hz may be deduced for TMP adsorbed on Brønsted acid sites of H-MOR and H-beta, respectively. A more intense downfield shift in $\delta^{31}\text{P}$ and a larger $J_{\text{P}-\text{H}}$ constant were observed for TMP adsorbed in H-MOR than those in H-beta, suggesting that the former possesses stronger acidity than the latter, in excellent agreements with their catalytic activities. It is indicative that the variations in $\delta^{31}\text{P}$ and $J_{\text{P}-\text{H}}$ values invoked by the ^{31}P -TMP NMR approach are useful for the evaluation of Brønsted acidity and catalytic activity in solid acid catalysts such as zeolites [43].

On the other hand, the ^1H -decoupled ^{31}P MAS spectra observed for H-MOR (Fig. 2.14A) and H-beta (Fig. 2.14B) invoking the ^{31}P -TMPO NR approach display multiple resonances with $\delta^{31}\text{P}$ in the range of 45–90 ppm. Accordingly, with the exception of the additional peak at 86.4 ppm observed for the TMPO/H-MOR system, both spectra revealed similar features, which could be deconvoluted into five overlapping components (peaks I–V). While peak V with $\delta^{31}\text{P}$ of ca. 45–50 ppm may be assigned due to physisorbed TMPO, the other peaks with $\delta^{31}\text{P}$ exceeding

55 ppm are attributed to TMPO adsorbed on Brønsted acid sites with different acidic strengths. As revealed by theoretical DFT calculations [18], a more intense interaction between TMPO and bridging hydroxyl proton may be inferred for Brønsted acid sites with stronger acidic strength. As a result, leading to a shift of ^{31}P -TMPO resonance towards downfield direction (i.e. towards a larger $\delta^{31}\text{P}$ value), an optimal $\delta^{31}\text{P}$ of 86.4 and 77.6 ppm was observed for TMPO adsorbed on H-MOR and H-beta, respectively, indicating that the former catalyst possesses Brønsted acidity with relatively higher acidic strength. Clearly, this notion coincides with that deduced from the aforementioned ^{31}P -TMP approach [43]. Thus, ^{31}P SSNMR of adsorbed phosphorus-containing probes represents a unique and sensitive technique for acidity characterization of solid acids. Accordingly, detailed information of acid features (viz., type, concentration, distribution, and strength of acid sites) in solid catalysts such as zeolites may be attained.

Transition metal-incorporated zeolites have been shown to be efficient catalysts for direct conversion of methane to benzene and toluene under nonoxidative conditions [45,46]. Bao and co-workers revealed that Mo/H-MCM-22 catalysts are desirable bifunctional catalysts for methane dehydroaromatization reaction [47]. In terms of catalytic performances of Mo/H-MCM-22 with varied metal loading, catalyst with a Mo loading of ca. 6 wt% was found to exhibit the optimal benzene selectivity, suppressed naphthalene yield, and prolonged catalyst life under a moderate methane conversion. Although both Brønsted and Lewis acid sites are capable of catalysing methane conversion reaction, active sites with higher acidic strengths are anticipated to play the dominant role.

To explore effects of incorporated Mo on acid properties, Huang *et al.* exploited ^{31}P -TMPO NMR approach to investigate Mo/H-MCM-22 catalysts with varied Mo loading [48]. As shown in Fig. 2.15, as many as 10 different resonance peaks, spanning over a $\delta^{31}\text{P}$ range of 31.0–83.0 ppm, were observed for the pristine MCM-22 and various $x\text{MoOM22IC}$ (x represents Mo loading; $x = 2\text{--}10$ wt%) catalyst samples. The notation for MoOM22IC represents the incorporation of molybdenum oxide (MO) on MCM-22 zeolite (M22) by impregnation method (I) and after a calcination (C) treatment. The two upfield peaks with lowest $\delta^{31}\text{P}$ of 41.3 and 31.4 ppm were unambiguously assigned due to physisorbed TMPO. In addition, the peak with $\delta^{31}\text{P}$ of 60.9 ppm was attributed to TMPO adsorbed on Lewis acid sites [29], whereas the other peaks were ascribed due to TMPO adsorbed on Brønsted acid sites. Upon progressive loading of Mo (<6 wt%), slight increases (ca. 1 ppm) in $\delta^{31}\text{P}$ of resonance peaks were observed, especially

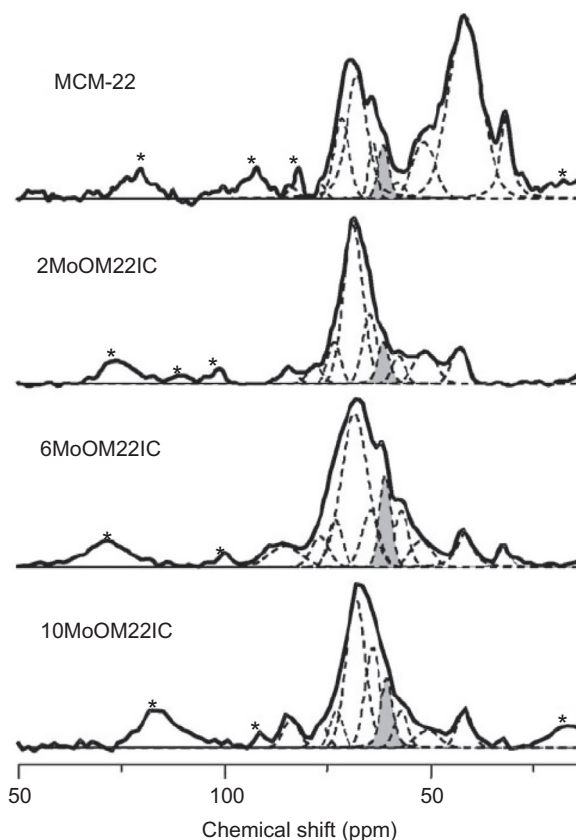


Figure 2.15 Solid-state ^{31}P MAS NMR spectra of TMPO adsorbed on parent MCM-22 and various calcined $x\text{MoOM22}$ samples ($x=2\text{--}10$ wt%) prepared by the impregnation method. The dashed lines represent Gaussian simulation results. The shaded peaks denote resonance arising from TMPO adsorbed on Lewis acid sites. Typically, a sample spinning rate of 10–12 kHz was used [48].

for those associated with acid sites with higher acidic strengths. As such, a mild increase in the overall acidic strength of MCM-22 with increasing Mo loading may be inferred for samples with $x < 6$ wt% (Fig. 2.15). By combining the ^{31}P NMR results with data obtained from elemental analyses by ICP, quantitative information regarding acid concentration may be deduced. Accordingly, a total Brønsted acidity amount of 0.470, 0.278, 0.263, and 0.203 mmol/g was derived for MCM-22, 2MoOM22IC, 6MoOM22IC, and 10MoOM22IC, respectively. A drastic decrease in both Brønsted and Lewis acidities upon immediate incorporation of Mo species onto MCM-22 may be inferred. For example, a respective decrease of ca.

41% and 94% in total Brønsted and Lewis acidities was found for the 2MoOM22IC catalyst compared to the parent MCM-22. However, only marginal decreases were observed when the Mo loading was increased from 2 to 6 wt%. Moreover, as the Mo loading was further increased to 10 wt%, considerable decrease in total acid concentration was observed.

It is noteworthy that the amounts of acid sites with highest acidic strengths (i.e. those with $\delta^{31}\text{P}$ of ca. 84 and 76 ppm) tend to increase at the expense of weaker acidity while increasing the Mo loading, reaching an optimal value at ca. 6 wt% loading. Nonetheless, further increasing the Mo loading exceeding 6 wt% led to notable decrease in the amount of strong acid sites. Thus, it is conclusive that the ^{31}P -TMPO NMR approach is capable of providing valuable information on the distribution and strength of acid sites, which in turn help to explain the peculiar catalytic performance of Mo/H-MCM-22 catalyst with a Mo loading of 6 wt% during methane dehydroaromatization reaction.

3.2.2 Metal Oxides and Mixed Metal Oxides

Nanostructured titanate materials, which can be fabricated with exotic morphologies (such as layered, nanosheet, nanotube, and nanorod), and their applications as solid acid catalysts have drawn considerable attentions in recent years [49,50]. It has been demonstrated that titanate nanotubes exhibit excellent catalytic activity for Friedel–Crafts alkylation of toluene with benzyl chloride at ambient temperature, surpassing that of layered titanates ($\text{H}_2\text{Ti}_3\text{O}_7$) and nanosheets ($\text{H}_{0.7}\text{Ti}_{1.825}\square_{0.175}\text{O}_4 \cdot \text{H}_2\text{O}$) having similar crystalline structures [51]. Again, the ^{31}P -TMPO NMR approach has been employed to elucidate correlations between catalytic reactivity and Brønsted acidity in these titanate nanomaterials [51]. For TMPO adsorbed on protonated titanate nanotubes, a distinct broad ^{31}P peak at ca. 65 ppm was observed, which may be attributed to the formation of TMPOH^+ species (Fig. 2.16). However, this peak tends to shift towards upfield direction (at ca. 60 ppm) when TMPO is adsorbed on layered titanates or titanate nanosheets, indicating that the latter two catalysts possess relatively weaker Brønsted acid strength. It is noteworthy that the $\delta^{31}\text{P}$ observed for TMPO adsorbed on titanate nanotubes (ca. 65 ppm) corresponds to acidic strength comparable to that of niobic acid, HY zeolite, and HTiNbO_5 nanosheet catalysts [52–54] but weaker than those of H-ZSM-5 (ca. 86 ppm). That layered titanates and titanate nanosheets exhibit similar $\delta^{31}\text{P}$ of adsorbed TMPO indicates that the amount of defect sites in titanate is irrelevant to its Brønsted acidity. In this context, the higher acidic strength observed for titanate nanotubes should be associated with lattice distortion caused

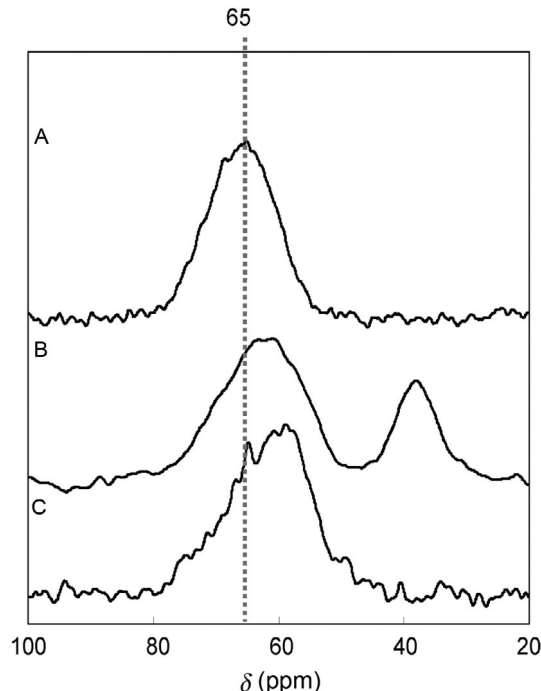


Figure 2.16 ^{31}P MAS NMR spectra of TMPO adsorbed on (A) titanate nanotubes, (B) $\text{H}_2\text{Ti}_3\text{O}_7$ nanosheets, and (C) $\text{H}_{0.7}\text{Ti}_{1.825}\square_{0.175}\text{O}_4\cdot\text{H}_2\text{O}$ nanosheets [51].

by the scrolling of lamellar titanate nanosheet, as also evidenced by results from Raman spectroscopy and DFT calculations [51].

Domen and co-workers also adopted the ^{31}P -TMPO NMR approach to characterize the acid properties of nanosheet aggregates prepared from protonated layered tungstates $\text{M}(\text{OH})\text{M}'$ ($\text{M} = \text{Nb}, \text{Ta}; \text{M}' = \text{Nb}, \text{W}$) [55]. As shown in Fig. 2.17, a broad resonance with overlapping features centring at ca. 60–75 ppm was observed for TMPO adsorbed on HTiNbO_5 , HNb_3O_8 , and HNbWO_6 nanosheets in addition to peaks responsible for physisorbed and crystalline TMPO ($\delta^{31}\text{P} < 50$ ppm). In the case of TMPO adsorbed on HTaWO_6 , an additional shoulder peak at ca. 84 ppm emerged along with the two main features at ca. 72 and 66 ppm, indicating the presence of very strong acid sites. In terms of acid strengths of these nanosheet catalysts, the following order may be inferred: $\text{HTaWO}_6 > \text{HNbWO}_6 > \text{HNb}_3\text{O}_8 > \text{HTiNbO}_5$. The same research group further adopted similar approach to probe acid properties of novel mesoporous oxide materials, namely, $\text{Nb}_x\text{W}_{(10-x)}$ [56]. As shown in Fig. 2.18, the main resonance peak of the adsorbed TMPO tends to shift towards

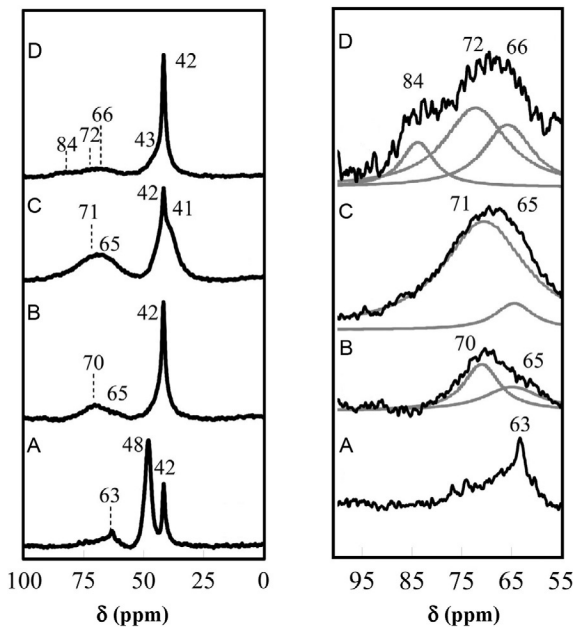


Figure 2.17 Left: Room-temperature ^{31}P MAS NMR spectra for TMPO adsorbed on various nanosheets aggregates: (A) HTiNbO_5 , (B) HNb_3O_8 , (C) HNbWO_6 , and (D) HTaWO_6 . All spectra were acquired with a MAS spinning rate of 10 kHz. Right: Expanded spectra [55].

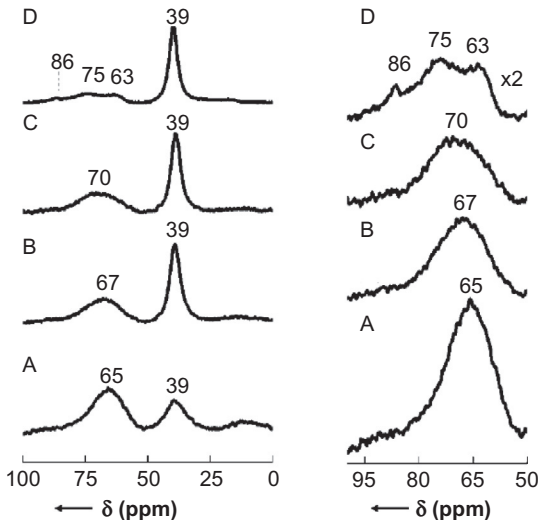


Figure 2.18 Left: Room-temperature ^{31}P MAS NMR spectra for TMPO (loading: 0.8 mmol per gram catalyst) adsorbed on mesoporous (A) Nb , (B) Nb_7W_3 , (C) Nb_5W_5 , and (D) Nb_3W_7 oxides. All spectra were acquired with a MAS spinning rate of 10 kHz. Right: Expanded spectra [56].

downfield direction from 67 ppm ($x=7$) to 70 ppm ($x=5$), indicating an enhanced acidic strength with decreasing loading of Nb. Moreover, a distinct small peak at 86 ppm was observed for TMPO adsorbed on Nb_3W_7 ($x=3$), revealing the presence of super acidity [18,56].

Among various mixed metal oxides, titania-based binary metal oxides such as $\text{TiO}_2\text{-SiO}_2$ and $\text{TiO}_2\text{-ZrO}_2$ have received much attention due to its unique acid/base and reduction/oxidation properties suitable for heterogeneous catalysis and wide bandgap desirable for photocatalytic applications [57,58]. In terms of their acid/base properties, bare TiO_2 is known to possess exclusively Lewis acidity, while bare SiO_2 exhibits only weak Brønsted acidity owing to silanol groups abundant on the surface. Nevertheless, the nature and origins of acidic sites on $\text{TiO}_2\text{-SiO}_2$ mixed oxides remain as debatable issues. As mentioned earlier, acidity characterization utilizing ^{31}P SSNMR of phosphorus-containing probe molecules may have different approaches. While TMPO probe is more sensitive to Brønsted sites with varied acidic strengths in solid acid catalysts, TMP is more suitable for probing Lewis acidity and hence capable of discriminating acid types, namely, Brønsted versus Lewis acid sites. Therefore, by combining the two different ^{31}P SSNMR approaches using TMP and TMPO probes, variations of acid sites in mesoporous $\text{TiO}_2\text{-SiO}_2$ mixed oxides with $\text{Ti/Si}=1$ before and after hydrogenation, denoted as mTS-1.0 and H-mTS-1.0, respectively, may be evaluated.

The ^{31}P NMR spectrum of TMPO adsorbed on mTS-1.0 revealed three main resonance peaks at 62.7, 57.1, and 44.2 ppm, which may be attributed to guest molecule adsorbed on Brønsted and Lewis acid sites and physisorbed TMPO, respectively (Fig. 2.19A). On the other hand, the ^{31}P spectrum of TMP adsorbed on mTS-1.0 showed two ^{31}P peaks at -5.8 and -35.5 ppm,

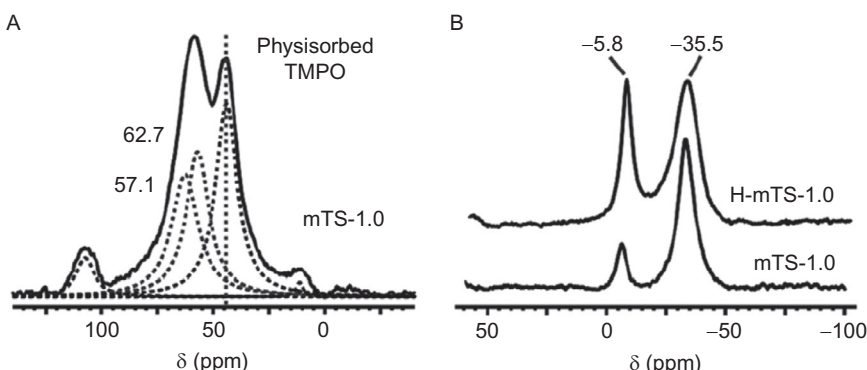


Figure 2.19 ^{31}P NMR of (A) TMPO adsorbed on mTS-1.0 and (B) TMP adsorbed on mTS-1.0 and H-mTS-1.0 mesoporous $\text{TiO}_2\text{-SiO}_2$ catalysts [59].

which may be assigned due to the presence of Brønsted and Lewis acid sites, respectively. It is noteworthy that TMP adsorbed on bare SiO_2 interactions between the probe molecule and the weak acidic surface $-\text{OH}$ groups tend to form hydrogen bonding, leading to ^{31}P NMR resonances at ca. -50 to -60 ppm. In this context, the signal at -5.8 ppm responsible for TMP adsorbed on mTS-1.0 and H-mTS-1.0 may be attributed to the presence of protonated adduct, namely, TMPh^+ , indicating the presence of much stronger Brønsted acidity in the $\text{TiO}_2\text{-SiO}_2$ (Fig. 2.19B). Moreover, the intensities of the signals at -5.8 and -35.5 ppm may be used to determine the relative concentration of Brønsted and Lewis acid sites in $\text{TiO}_2\text{-SiO}_2$. As may be seen in Fig. 2.19B, a notable increase in intensity of the peak at -5.8 ppm responsible for Brønsted acidity was observed for H-mTS-1.0 compared to mTS-1.0, while no change for the peak at -35.5 ppm was found. It is indicative that hydrogenation treatment promotes enhancement in the concentration of Brønsted acid sites in $\text{TiO}_2\text{-SiO}_2$ due to partial reduction of Ti(IV) to Ti(III) while keeping Lewis acidity practically unchanged [59].

The acid properties of sulphated TiO_2 (denoted as $\text{SO}_4^{2-}/\text{TiO}_2$) have also been investigated by means of the ^{31}P -TMPO NMR approach [22]. As shown in Fig. 2.20A, the ^{31}P MAS NMR spectrum of TMPO adsorbed on pristine TiO_2 revealed a main resonance at 48 ppm due to physisorbed TMPO and a much weaker broad signal centring at ca. 59 ppm, which may

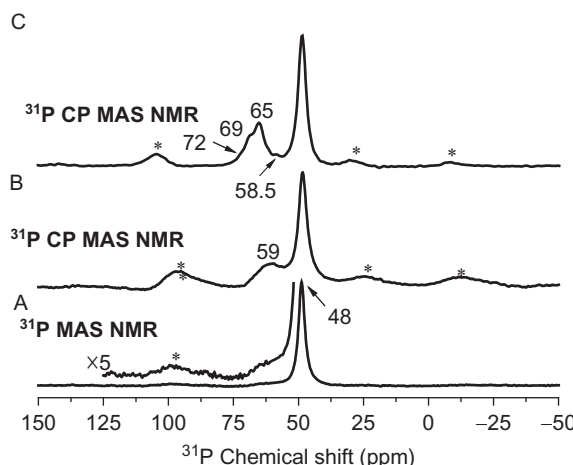


Figure 2.20 ^{31}P (A) MAS and (B) CP MAS NMR spectra of TMPO adsorbed on TiO_2 and (C) MAS NMR spectrum of TMPO adsorbed on $\text{SO}_4^{2-}/\text{TiO}_2$. Asterisks denote spinning sidebands [22].

be attributed to TMPO adsorbed on Lewis acid sites. The assignment of the latter peak was further confirmed by additional ^{31}P CP MAS NMR experiment to eliminate undesirable artefacts originating from spinning sidebands. As a result, the resonance signal at 59 ppm was greatly enhanced ([Fig. 2.20B](#)). For TMPO adsorbed on $\text{SO}_4^{2-}/\text{TiO}_2$, apart from the signals of physisorbed TMPO (48 ppm) and TMPO adsorbed on Lewis acid sites (58.5 ppm), three signals at 65, 69, and 72 ppm were also observed ([Fig. 2.20C](#)), which may be ascribed due to TMPO adsorbed on three types of Brønsted acid sites with varied acidic strengths.

Sulphated zirconia ($\text{SO}_4^{2-}/\text{ZrO}_2$; SZ) is an environmentally friendly and a practical solid acid catalyst that has been extensively used for low-temperature conversion of hydrocarbons. Nonetheless, SZ is also known as a strong acidic catalyst vulnerable to deactivation [[60](#)]. This drawback is normally circumvented by adding suitable amount of metal promoter, such as Pt, Al, Ga, Fe, or Mn [[61,62](#)]. However, the acid properties of SZ and metal-promoted SZ (denoted as M/SZ) have not yet been clarified. Liu and co-workers adopted the ^{31}P -TMPO NMR approach to characterize the acid features (type, concentration, and strength) of various SZ and M/SZ catalysts [[26](#)]. As shown in [Fig. 2.21](#), the ^{31}P NMR spectrum of TMPO adsorbed on the dehydrated parent ZrO_2 revealed four distinct resonance peaks at 62, 53, 41, and 34 ppm. The latter two peaks with $\delta^{31}\text{P}$ lower than 50 ppm can be unambiguously assigned due to physisorbed TMPO, while the former two peaks (62 and 53 ppm) may be attributed to TMPO adsorbed on Lewis acid sites, as confirmed by additional experiments performed on partially hydrated samples ([Fig. 2.21](#)). Unlike the parent ZrO_2 sample, the TMPO-loaded SZ- x N samples ($x = 0.5, 1.0$, and 2.0, where x represents the concentration of sulphuric acid added during the sulphation treatment) all reveal four distinct ^{31}P resonance peaks at 90, 87, 68, and 63 ppm ([Fig. 2.21](#)). Assorted data are depicted in [Table 2.3](#). It is indicative that coexisting Lewis (at 90 and 63 ppm) and Brønsted (at 87 and 68 ppm) acid sites were present in SZ- x N samples. In particular, the emergences of the strong Lewis acid sites (at 90 ppm) as well as Brønsted acid sites with strong (87 ppm) and medium (68 ppm) acidic strengths that took place mostly at the expanses of the weak Lewis acidity originally existed in the pristine ZrO_2 , particularly the one with weaker strength (at 53 ppm), which diminishes upon sulphation treatment. Moreover, a maximum Brønsted, Lewis, and total acidities were found on sample sulphated with a sulphuric acid concentration (x) of 1.0 N.

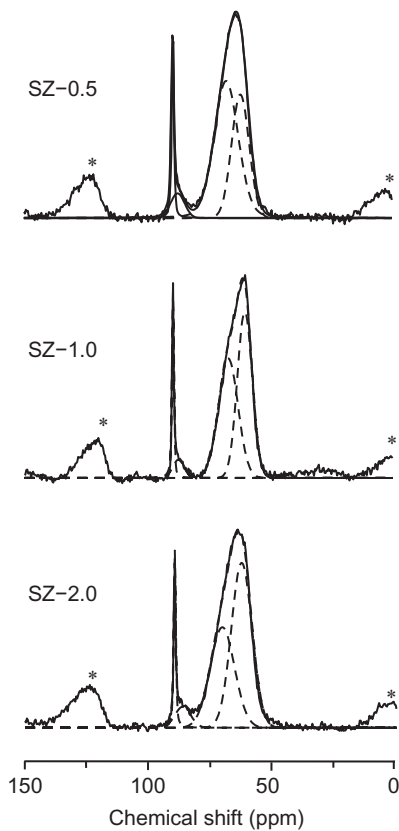


Figure 2.21 ^{31}P MAS NMR spectra of TMPO adsorbed on dehydrated SZ- $x\text{N}$ ($x = 0.5, 1.0$, and 2.0) prepared with varied sulphur contents. The dashed curves represent spectral simulation results and the asterisks denote spinning sidebands (spinning rate 12 kHz) [26].

Upon incorporating ca. 1.0 wt% of metal (Al, Ga, and Fe) onto the SZ-1.0N catalyst, both TMPO-loaded Al/SZ and Ga/SZ samples exhibit a total of eight ^{31}P resonances (Fig. 2.22A), in which four of them have identical $\delta^{31}\text{P}$ with those found for the nonpromoted SZ-1.0N. By the same token with the methodology illustrated earlier, identification of acid types may be accomplished by performing additional experiments on hydrated samples (Fig. 2.22B). Accordingly, the presences of extra Brønsted (76 and 65 ppm) and Lewis (73 and 53 ppm) acid sites in M/SZ may be inferred, as summarized in Table 2.3. Note that these additional peaks tend to span over a wide range (from weak to medium) of acidic strengths, occurred mostly at the disposals of the strongest Lewis acid sites (at 90 ppm) and

Table 2.3 ^{31}P MAS NMR chemical shift assignments and distribution of acid sites for various SZ and M/SZ samples loaded with TMPO probe molecule [26]

Sample	Chemical shift (ppm) ^{a,b}								Acid amount (mmol/g cat.) ^c					
	[99]	[90]	87	76	[73]	68	65	[62]	[53]	P ^c	Brønsted	Lewis	Total	B/L (%)
ZrO ₂	—	—	—	—	—	—	—	50.3%	49.7%	✓	—	—	—	—
SZ-0.5N	—	7.9% (0.003)	5.4% (0.002)	—	—	53.3% (0.023)	—	33.4% (0.015)	—	—	0.025	0.018	0.043	1.39
SZ-1.0N	—	7.4% (0.012)	3.7% (0.006)	—	—	43.2% (0.071)	—	45.7% (0.075)	—	—	0.077	0.087	0.164	0.89
SZ-2.0N	—	6.0% (0.005)	5.1% (0.004)	—	—	37.2% (0.028)	—	51.7% (0.039)	—	—	0.032	0.044	0.076	0.73
Al/SZ	—	5.3% (0.008)	4.3% (0.006)	2.8% (0.004)	3.1% (0.005)	9.7% (0.015)	15.3% (0.023)	55.8% (0.084)	3.7% (0.006)	—	0.048	0.103	0.151	0.47
Ga/SZ	—	4.1% (0.005)	5.5% (0.007)	3.5% (0.005)	7.8% (0.010)	14.4% (0.019)	41.9% (0.054)	20.0% (0.026)	2.8% (0.004)	—	0.085	0.045	0.130	1.89
Fe/SZ	4.5% (0.013)	—	6.3% (0.018)	—	—	12.9% (0.038)	13.7% (0.040)	27.0% (0.079)	35.6% (0.105)	✓	0.096	0.197	0.293	0.49

^aFor comparison, simulation results (see text) obtained for various samples representing TMPO adsorbed on Brønsted and/or Lewis (denoted by chemical shift values in brackets) acid sites with practically the same chemical shift (i.e. similar acid strengths) are aligned in the same column.

^bFor SZ- x N ($x=0.5, 1.0$, and 2.0) and M/SZ (M=Al, Ga, and Fe) samples, data denote relative concentration of acid sites (%), whereas data in parentheses represent acid concentration (± 0.002 mmol/g cat.) of the corresponding acid site, as derived from elemental analyses by ICP-MS.

^cResonance peaks with chemical shift lower than 50 ppm, which arise from physisorbed TMPO, were excluded during derivations of acid amount.

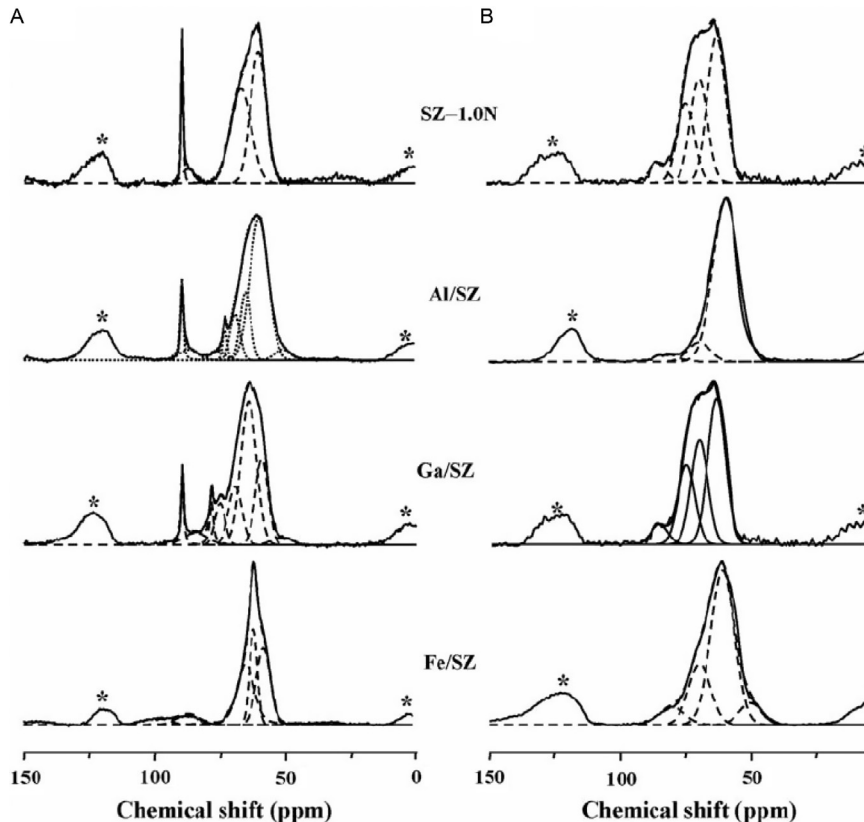


Figure 2.22 ^{31}P MAS NMR spectra of TMPO adsorbed on dehydrated M/SZ (M = Al, Ga, and Fe) (A) before and (B) after hydration treatment (for 1 h). The dashed curves represent spectral simulation results and the asterisks denote spinning sidebands (spinning rate 12 kHz) [26].

medium Brønsted acid sites (at 68 ppm) in SZ-1.0N. For the Fe/SZ catalyst, formations of very strong (99 ppm) and very weak (53 ppm) Lewis acid sites that are accompanied by the notable increase in strong (87 ppm) and additional weak (65 ppm) Brønsted acid sites were observed, mostly at the collaborative expanses of the strong (90 ppm) and weak (62 ppm) Lewis and medium Brønsted (68 ppm) acid sites of its parent SZ-1.0N. Obviously, by the incorporation of different metal species onto SZ not only resulted in formation of new Brønsted and Lewis acid sites with varied acidic strengths but also leads to variations in concentration among different acid sites, which are anticipated to have considerable impact to their catalytic activity and selectivity.

3.2.3 Heteropolyacids

HPAs, especially those with Keggin-type structures, have been extensively employed as solid acid catalysts and photocatalysts in various homogeneous solutions, liquid–solid, and gas–solid heterogeneous reactions due to their strong acidity. Figure 2.23 displays the ^{31}P MAS NMR spectra of varied amount of TMPO adsorbed on 12-molybdophosphoric acid ($\text{H}_3\text{PMo}_{12}\text{O}_{40}$; HPMo) with varied loading. The ^{31}P resonances in the range of -5 to -10 ppm were due to the $\text{PMo}_{12}\text{O}_{40}^{3-}$ polyanions [64,65]. Upon adsorption of TMPO probe molecule, broad resonance peaks in the $\delta^{31}\text{P}$ range of 80 – 90 ppm were observed (Fig. 2.23) [63]. Further spectral analyses revealed that these peaks may be deconvoluted into five resonances centred at 89.9 , 87.5 , 86.2 , 83.7 , and 81.2 ppm. On the basis of DFT calculations, $\delta^{31}\text{P}$ can be predicted theoretically for various TMPO/HPMo adsorption complexes. The formal three peaks at 89.9 , 87.5 , and 86.2 ppm may be assigned to one TMPO adsorption complex per Keggin

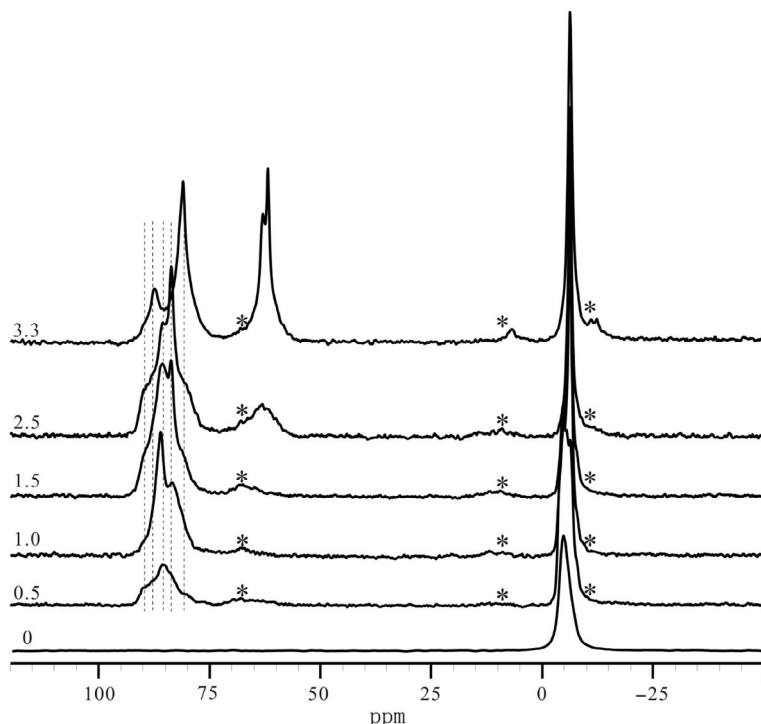


Figure 2.23 ^{31}P MAS NMR spectra of bare HPMo and TMPO/HPMo samples with varied TMPO loading ranging from 0.5 to 3.3 TMPO/KU. Prior to the NMR experiments, each TMPO-loaded sample was subjected to baking treatment at 473 K for 8 h [63].

unit (KU), that is, TMPOH^+/KU , whereas the latter two signals at 83.7 and 81.2 ppm may be ascribed to two TMPOH^+ complexes in one KU, that is, $(\text{TMPOH}^+)_2/\text{KU}$. Nevertheless, as the TMPO loading exceeds ca. 2.5 TMPO/KU, an additional broad signal centring at ca. 63 ppm was observed. As shown in Fig. 2.24, additional $^{31}\text{P}\{\text{H}\}$ LG-CP HETCOR experiments [36] were used to further validate interactions between the TMPO (guest adsorbate) molecules and Brønsted acid sites in HPMo (host adsorbent). Such 2D multinuclei technique represents a direct approach to probe correlations between the local environments of ^1H and ^{31}P nuclei. The cross peaks that correlate ^{31}P resonances at ca. 80–90 ppm and ^1H resonances at ca. 6–8 (Fig. 2.24A) and 9–13 (Fig. 2.24B) ppm should be originated from one TMPO adsorbed on various protonic sites (i.e. TMPOH^+) in HPMo with varied acidic strengths. Whereas, the cross peaks that correlate the ^{31}P and ^1H resonances at ca. 60–65 ppm and ca. 15.5–16.5 ppm, respectively, should be due to the presence of $(\text{TMPO})_2\text{H}^+$ adsorption complexes in which the probe molecules are in close proximities with one and other (Fig. 2.24C). However, the cross peaks associated with ^{31}P resonances at ca. 80–90 and 60–65 ppm and ^1H resonances at ca. 1.5–3.5 ppm should be arising from intramolecular interactions between the methyl protons and the ^{31}P nucleus of the TMPO and hence are irrelevant to the distribution of protonic sites in HPMo.

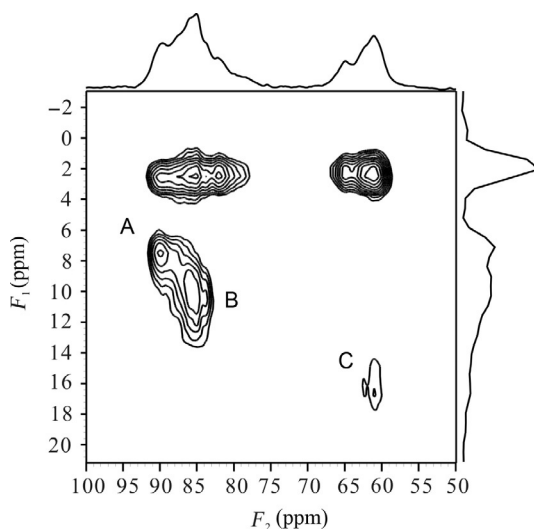


Figure 2.24 $^{31}\text{P}\{\text{H}\}$ LG-CP HETCOR spectrum of TMPO adsorbed on HPMo sample with a loading of 2.5 TMPO/KU. Prior to the NMR experiment, the TMPO-loaded sample was subjected to baking treatment at 473 K for 8 h [63].

It is noteworthy that the adsorption behaviour obtained from the TMPO/HPMo system is somewhat different from that of the TMPO adsorbed on 12-tungstophosphoric acid ($\text{H}_3\text{PW}_{12}\text{O}_{40}$; HPW) system. The investigation on the latter system showed that $(\text{TMPO})_2\text{H}^+$ complexes tend to diminish when the TMPO-loaded HPW samples were subjected to baking treatment ($T_b \geq 423$ K), leaving only homogeneously distributed adsorption complex in the form of $(\text{TMPOH}^+)_3/\text{KU}$ in HPW (see Fig. 2.25) [66]. This is clearly not the case for the TMPO/HPMo system, for which adsorption complexes are in the form of $(\text{TMPOH}^+)_n/\text{KU}$. ($n=1, 2$) and $(\text{TMPO})_2\text{H}^+$ were also present in addition to the $(\text{TMPOH}^+)_3/\text{KU}$, even after a thorough sample pretreatment at $T_b = 473$ K [66]. Therefore, it is

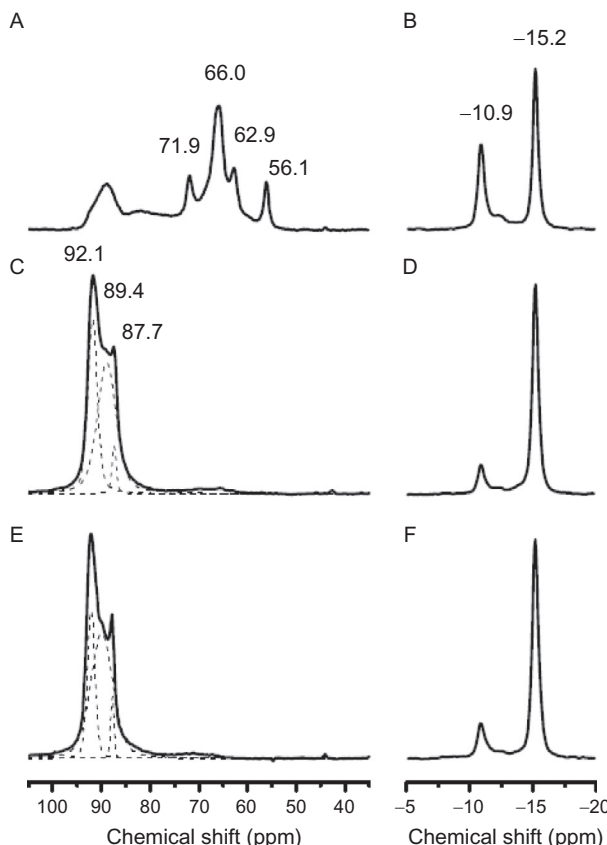


Figure 2.25 Left: ^{31}P MAS NMR spectra of protonated TMPO adducts arising from TMPO adsorbed on HPW (loading 2.5 TMPO/KU). Right: ^{31}P signal corresponding to $\text{PW}_{12}\text{O}_{40}^{3-}$ polyanions. Prior to the NMR experiments, the sample was subjected to baking treatment at (A, B) 373 K, (C, D) 423 K, and (E,F) 473 K for 6 h [66].

hypothesized that HPMo has a relatively weaker pseudoliquid characteristic compared to that of HPW, making the TMPO probe molecules more difficult to diffuse within its secondary structure. Such discrepancy in acid properties observed for HPMo and HPW may be ascribed due to differences in the electronic configurations of Mo ($4d_55s_1$) and W ($5d_46s_2$), although these HPAs have a similar crystalline structure.

3.2.4 Functionalized Carbon Materials

Bifunctional carbon–silica composite materials (CSM), which have been shown to be efficient catalysts for conversion of sugars, are normally constructed by porous silicas (such as mesoporous MCM-41 molecular sieve) tucked with porous carbon matrix [67]. The ^{31}P -TMPO NMR approach was used to probe the acid strength of CSM catalysts [67]. The authors attributed the ^{31}P resonances with $\delta^{31}P$ within the range of 40–70 ppm to the presence of weakly acidic oxygen-containing surface groups on the carbonized material. To avoid interference arising from physisorbed and crystalline TMPO, a TMPO loading under the estimated stoichiometric amount was adopted. As a result, no ^{31}P resonance at 41 ppm was found, indicating that crystalline TMPO was indeed absent. Consequently, two ^{31}P resonances were observed for the TMPO-loaded CSM sample posttreated at 573 K. The authors ascribed the main peak (at ca. 45 ppm) and the weak shoulder peak (at ca. 60 ppm) to TMPO adsorbed on weak and strong acid sites in CSM, respectively. The broadening of the ^{31}P resonance observed for the posttreated samples was attributed to heterogeneous distribution of acid sites with varied acidic strengths in the catalyst. The Brønsted acidity observed for CSM mainly arises from the surface functional groups such as phenols, anhydrides, and carboxylic acids in carbon matrix, thus exhibiting an overall acidic strength much weaker than that of typical zeolites. Nonetheless, the absence of strong Brønsted acid sites serves to avoid the occurrence of undesirable side reactions. Moreover, the strength and concentration of Brønsted acid sites in CSM may readily be controlled by varying the carbon deposition content, pyrolysis temperature, and thermal posttreatment conditions.

Mesoporous poly(divinylbenzene) (PDVB)-based solid acids, such as PDVB- SO_3H - SO_2CF_3 prepared by grafting of strong electron withdrawing group of SO_2CF_3 onto the network of mesoporous PDVB- SO_3H , have been demonstrated to exhibit excellent catalytic activities during biomass transformation towards transesterification to biodiesel and depolymerization of crystalline cellulose to sugars. To unravel the correlation between

acid property and reaction activity, Liu *et al.* adopted the ^{31}P -TMPO NMR approach to characterize the distribution and strength of acid sites in PDVB- SO_3H and PDVB- $\text{SO}_3\text{H}-\text{SO}_2\text{CF}_3$ catalysts [68]. As shown in Fig. 2.26A, the ^{31}P MAS NMR spectrum of TMPO adsorbed on PDVB- SO_3H shows two resonances with $\delta^{31}\text{P}$ of 72 and 80 ppm with a relative peak area (concentration) of 40% and 60%, respectively. These two ^{31}P resonances may be attributed unambiguously to TMPO adsorbed on acid sites of PDVB- SO_3H with different acidic strengths, forming TMPOH^+ complexes with varied extents of protonation. Upon further treatment of PDVB- SO_3H by HSO_3CF_3 , notable increase in Brønsted acidic strength was observed for the PDVB- $\text{SO}_3\text{H}-\text{SO}_2\text{CF}_3$ catalyst, leading to a more homogeneously distributed acid sites, as revealed by the singlet peak with $\delta^{31}\text{P}$ of 83 ppm in Fig. 2.26B. Furthermore, based on the correlation between DPE and ^{31}P CS attained for the ^{31}P -TMPO NMR approach in Eq. (2.4), DPE value corresponding to $\delta^{31}\text{P}$ of 72, 80, and 83 ppm should be ca. 284, 264, and 256 kcal/mol, respectively. Apparently, the acidic strengths in PDVB- SO_3H were dramatically enhanced through the treatment by the electron withdrawing CF_3 groups, thus more favourable for enhancing the catalytic activity of the catalyst.

Similar treatment by SO_3H may also be applied to modify the surface of porous carbon materials to facilitate active functional moieties desirable for acid-catalysed hydrophobic reactions. As a result, the surface SO_3H groups

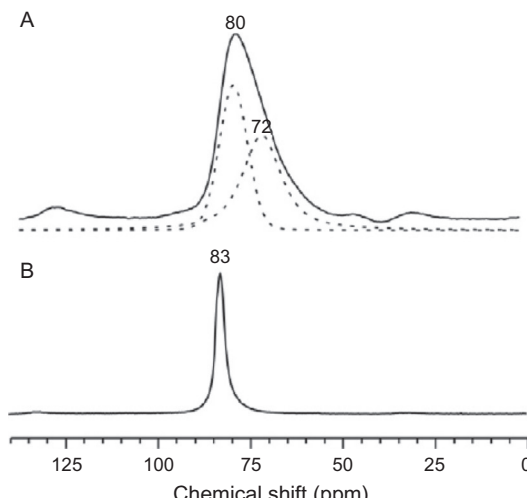


Figure 2.26 Solid-state ^{31}P MAS NMR spectra of TMPO adsorbed on (A) PDVB- SO_3H and (B) PDVB- $\text{SO}_3\text{H}-\text{SO}_2\text{CF}_3$ solid acid catalysts [68].

may be readily accessed by hydrophobic reactants, leading to the high catalytic performance observed for such functionalized carbons. Hara and co-workers utilized the ^{31}P -TMPO NMR approach to investigate acid properties of functionalized mesoporous carbon-based solid acids, namely, CAC, RF-773, and RF-973, prepared by postsynthesis sulphonation treatment. Among them, CAC represents cellulose-derived bulky amorphous carbon-bearing $-\text{SO}_3\text{H}$ and phenolic $-\text{OH}$ groups; RF-773 and RF-973 samples were amorphous carbon with different amounts of phenolic $-\text{OH}$ groups, the former having a higher amount than the latter. The ^{31}P resonance at 83 ppm observed in Fig. 2.27A for the CAC material was attributed to TMPO adsorbed on SO_3H groups. On the other hand, the corresponding spectrum for RF-773 revealed three distinct signals at 78, 63, and 41 ppm (Fig. 2.27B), which were assigned due to TMPO adsorbed on acidic $-\text{SO}_3\text{H}$, phenolic $-\text{OH}$, and self-aggregated TMPO, respectively. In the case of RF-973, however, only the signal of self-

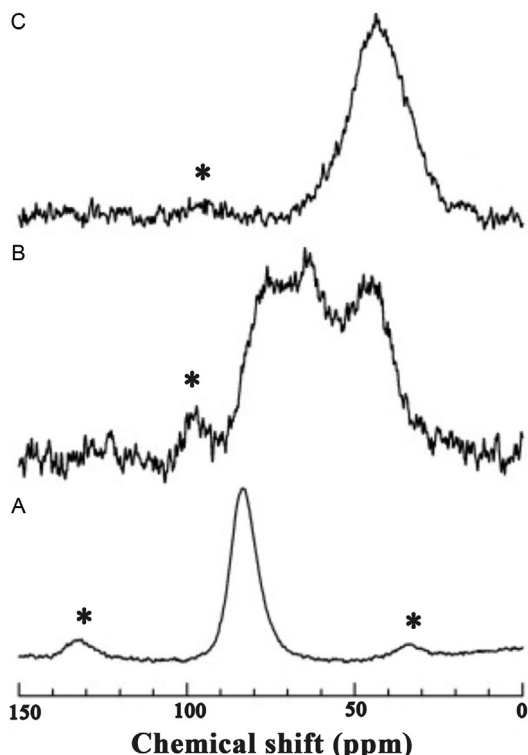


Figure 2.27 ^{31}P MAS NMR spectra of TMPO adsorbed on (A) CAC, (B) RF-773, and (C) RF-973 after TMPO adsorption. The asterisks denote spinning sidebands [69].

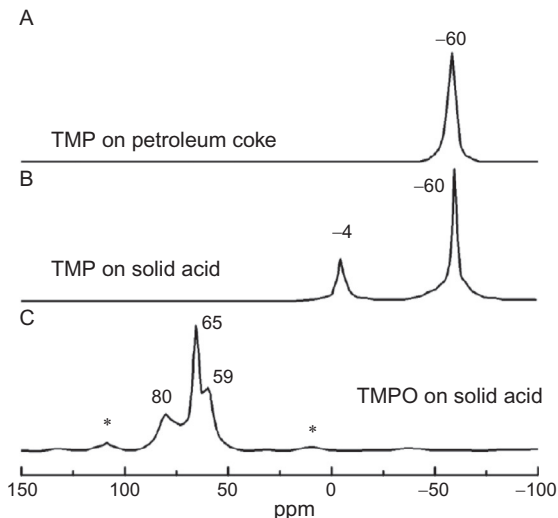


Figure 2.28 ^1H -decoupled ^3P MAS NMR spectra of TMP adsorbed on (A) petroleum coke, (B) solid acids, and (C) TMPO adsorbed on solid acid. The asterisks denote spinning sidebands [70].

aggregated TMPO (41 ppm) was observed (Fig. 2.27C), despite of the fact that vibrational bands responsible for $-\text{SO}_3\text{H}$ group were evident in the IR spectrum. The authors hypothesized that this may be due to the $-\text{SO}_3\text{H}$ and phenolic $-\text{OH}$ groups in RF-973 that were inaccessible to the TMPO probe molecule. Consequently, a null catalytic activity was observed for the RF-973 catalyst during α -methylstyrene dimerization reaction [69].

Petroleum cokes are one of the vast by-products in petrochemical industry. To salvage these petroleum cokes, it is common to invoke KOH activation and/or H_2SO_4 sulphonation treatment to incorporate functional groups such as $-\text{OH}$, $-\text{COOH}$, and $-\text{SO}_3\text{H}$ onto the carbonaceous substrates. As a result, surface-functionalized petroleum cokes have been considered as novel solid acid catalysts. Zeng *et al.* studied the acid properties of functionalized petroleum cokes by means of the ^{31}P SSNMR of adsorbed TMP and TMPO and examined their catalytic performances during esterification of oleic acid with methanol [70]. As shown in Fig. 2.28A, the ^{31}P spectrum obtained for TMP adsorbed on the unmodified petroleum coke material revealed only a single peak at -60 ppm, which may be assigned due to physisorbed TMP. This indicates that neither Lewis nor Brønsted acid sites were present in the pristine petroleum cokes. Whereas two ^{31}P resonance peaks at -4 and -60 ppm were observed for TMP adsorbed on petroleum coke after the KOH/ H_2SO_4 treatment (Fig. 2.28B), the presence of the

new peak at -4 ppm indicates that the chemical activation and sulphonation treatment provoked the formation of Brønsted acid sites in the solid catalyst. On the other hand, three distinct ^{31}P resonances at 59 , 65 , and 80 ppm were observed by adopting the ^{31}P -TMPO NMR approach (Fig. 2.28C), which were ascribed to TMPO adsorbed on Brønsted acid sites with varied acidic strengths. Together with the results obtained from FTIR experiments and theoretical calculations, three types of moieties on the solid acid were identified, namely, weak ($-\text{OH}$), media ($-\text{COOH}$), and strong ($-\text{SO}_3\text{H}$) acidic functional groups. Thus, the resonances at 59 , 65 , and 80 ppm were assigned to TMPO adsorbed on the $-\text{OH}$, $-\text{COOH}$, and $-\text{SO}_3\text{H}$ groups on the surfaces of the modified petroleum cokes, respectively [70].

3.2.5 Commercial Catalysts

Commercial solid acid catalysts are mostly in the form of granular catalyst–binder extrudates in order to sustain their physicochemical and catalytic properties over the long-term catalytic cycles. Most commercial catalysts are commonly formulated by a certain type of zeolite catalyst with a desirable amount of alumina or silica binder and eventually extruded to form catalyst particles of various shapes and sizes [71]. Nonetheless, detailed information on acid properties of such catalyst mixture (especially in the case of commercial catalysts) is normally deficient in the literatures. Presumably, solid interactions between zeolite and binder materials may occur through intimate contact, which in turn may alter the acidity and catalytic properties of the original zeolite catalyst [72]. Moreover, the formation of carbonaceous residues (or cokes) during catalytic reaction is one of the major concerns from the industrial operation perspective. Since coking is a shape-selective reaction [73], the presence of binder, therefore, may alter the deactivation rate of the zeolite catalyst. It is well known that while acidity plays a key role during catalytic reactions, coking is the primary cause for catalyst deactivation. It was found that cokes tend to deposit on the acid sites located in the intracrystalline voids of the zeolitic catalyst during reaction and hence should be responsible for the decline in catalytic activity [74].

Liu and co-workers studied the effects of binder, coking, and regeneration on the acid properties of a commercial H-MOR catalyst during toluene disproportionation reaction [75]. The authors utilized ^{31}P SSNMR of adsorbed TMPO and TBPO for acidity characterization of various fresh, spent, and regenerated catalysts. As shown in Fig. 2.29, three resonance peaks with $\delta^{31}\text{P}$ at 68 , 56 , and 49 ppm were observed when TMPO was adsorbed on $\gamma\text{-Al}_2\text{O}_3$ binder material. While the peak at 49 ppm was

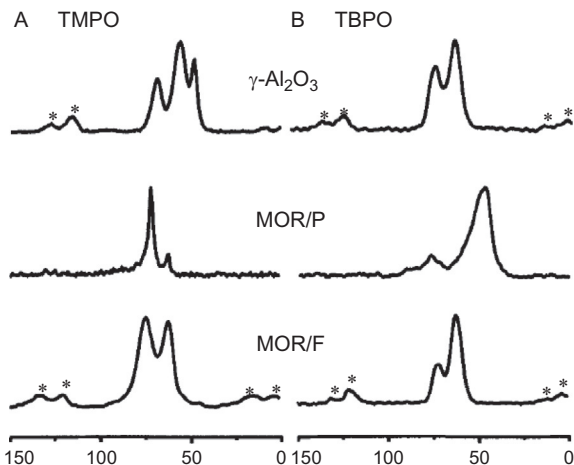


Figure 2.29 ^{31}P MAS NMR spectra of (A) TMPO and (B) TBPO adsorbed on various samples. The spinning sidebands are indicated by asterisks [75].

unambiguously assigned due to physisorbed TMPO, the other two down-field peaks were attributed to TMPO absorbed over two different Lewis acid sites. Since the pore size of the $\gamma\text{-Al}_2\text{O}_3$ binder (ca. 5 nm) is surely large enough to accommodate TBPO probe molecule (kinetic diameter (KD) 0.82 nm), three characteristic peaks at 74, 63, and 58 ppm were also observed for the TBPO/ $\gamma\text{-Al}_2\text{O}_3$ system, similar to that of TMPO/ $\gamma\text{-Al}_2\text{O}_3$. Besides the physisorbed TMPO, the ^{31}P spectra obtained from parent MOR zeolite (denoted as MOR/P) and fresh commercial catalyst (denoted as MOR/F) samples revealed additional signals ($\delta^{31}\text{P} > 74$ ppm) corresponding to Brønsted acid sites in the MOR zeolite. On the other hand, for TBPO adsorbed on MOR/P, the majority of the probe molecules were adsorbed on the extracrystalline surfaces of the zeolite. Note that the presence of $\gamma\text{-Al}_2\text{O}_3$ binder in MOR/F slightly broadens the resonance peaks and to some extent alters the relative concentrations of the weaker acid sites. Other than that, key features of Brønsted (from MOR/P) and Lewis acid sites (from $\gamma\text{-Al}_2\text{O}_3$) from their respective origins were largely preserved in mixture catalyst (MOR/F).

Figure 2.30 displays ^{31}P NMR spectra of TMPO and TBPO adsorbed on fresh commercial catalyst (MOR/F), various spent catalysts (MOR/C- x ; x represents coke content in wt%), and a regenerated catalyst (MOR/R). As summarized in Table 2.4, up to six resonances with $\delta^{31}\text{P}$ at 89, 80, 74, 68, 62, and 56 ppm were observed for TMPO adsorbed on the MOR/F sample.

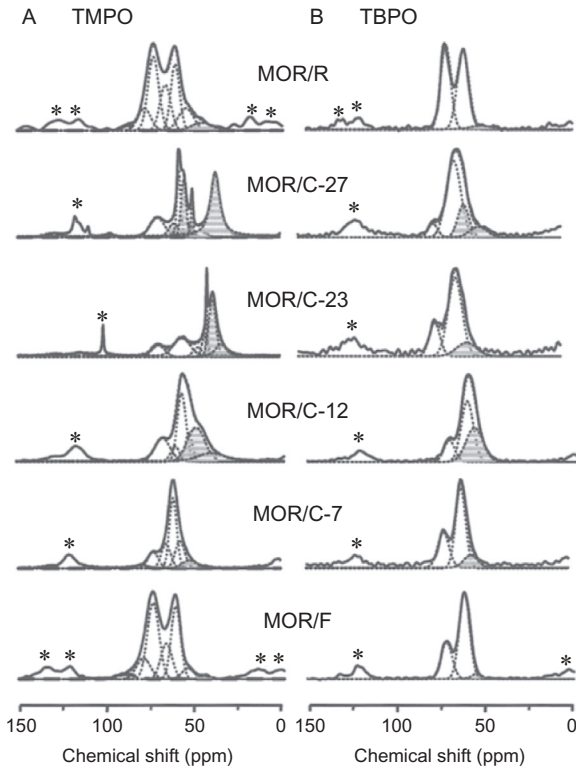


Figure 2.30 ^{31}P MAS NMR spectra of (A) TMPO and (B) TBPO adsorbed on fresh (MOR/F), regenerated (MOR/R), and various coked (MOR/C) samples. The dashed curves represent simulation of resonance peaks by Gaussian deconvolution method. Shaded peaks denote contributions from physisorbed adsorbates and the spinning sidebands are indicated by asterisks [75].

Among them, peaks at 68 and 56 ppm were attributed to the presence of Lewis acidity originated from the $\gamma\text{-Al}_2\text{O}_3$ binder, while the other peaks were assigned to Brønsted acid sites with varied acidic strengths. It is noted that, unlike TBPO that can only probe external acid sites, TMPO (0.55 nm) may be accommodated by the 12-MR or MOR zeolite and hence capable of probing both internal acidity and external acidity [75]. As such, the results depicted in Table 2.4 for the ^{31}P -TMPO approach are valid as far as the overall acid concentration is concerned. On the other hand, notable decreases in Brønsted acidity (especially those corresponding to peaks with $\delta^{31}\text{P}$ at 89 and 80 ppm) were observed during initial stage of reaction. This indicates that cokes tend to preferentially deposit on strongest acid sites during early time on stream.

Table 2.4 Assignments of ^{31}P NMR chemical shifts and distribution of acid sites for fresh, coked, and regenerated commercial H-mordenite samples loaded with TMPO probe molecule [75]

Sample	^{31}P NMR chemical shift versus acid concentration (ppm)					
	89	80	74	68	62	56
MOR/F	3.6 (0.014)	11.6 (0.044)	35.9 (0.135)	16.3 (0.061)	27.4 (0.103)	5.2 (0.020)
MOR/C-7	—	2.6 (0.006)	13.9 (0.031)	19.1 (0.043)	42.7 (0.096)	21.7 (0.049)
MOR/C-12	—	—	5.2 (0.016)	27.5 (0.084)	16.3 (0.050)	51.0 (0.156)
MOR/C-23	—	—	—	34.3 (0.007)	—	65.7 (0.143)
MOR/C-27	—	—	—	35.1 (0.117)	—	64.9 (0.216)
MOR/R	2.3 (0.007)	11.1 (0.035)	31.2 (0.098)	19.5 (0.061)	22.8 (0.071)	13.1 (0.041)

Values represent relative concentration of acid sites (%). Values in parentheses denote the acid amount of each site ($\pm 0.002 \text{ mmol/g catalyst}$).

As shown in Fig. 2.30 and Table 2.4, a progressive diminishing of the ^{31}P NMR resonances at downfield with increasing coke content (or duration of reaction) was evident, revealing a progressive inactivation of Brønsted acid sites. Note that such progressive decrease in Brønsted acidity is accompanied by a progressive increase in the amount (but not strength) of Lewis acidity. It was found that, as the catalyst coke content exceeds ca. 23 wt% (which corresponding to a time on stream of 40 days), the ^{31}P resonances associated with Brønsted acidity were mostly deactivated, while the concentration of Lewis acidity (peaks at 68 and 56 ppm) prevailed to sustain the toluene disproportionation reaction (at least up to 400 days, in case of MOR/C-27). Moreover, it is noteworthy that the majority of acid sites may be recovered upon a simple regeneration treatment, as can be seen by comparing results obtained from the MOR/R and MOR/F samples. Therefore, on the basis of such *ex situ* study using the ^{31}P -TMPO NMR approach, detailed variations of acid sites with reaction time can readily be pursued. Such approaches for acidity characterization should be valuable for the assessment of commercial catalysts.

3.3. Location, Distribution, and Spatial Proximity of Acid Sites

The location and distribution (e.g. internal vs. external) of acid sites may also play a role during catalytic reaction and thus are also crucial for the design and practical applications of solid acid catalysts. As mentioned earlier, the KD of TMPO is ca. 0.55 nm, which is comparable to the pore aperture of typical 10-MR (pore size ca. 0.60 nm) zeolites such as ZSM-5. However, the sizes of its analogous such as TEPO (KD ca. 0.60 nm), TBPO (KD ca. 0.82 nm), and TOPO (KD ca. 1.10 nm) are too large to penetrate into the channels/pores of 10-MR zeolites and hence can merely probe acid sites located on extracrystalline surfaces [24,25]. In this regard, acid sites in intracrystalline and on extracrystalline surfaces of different porous catalysts may be probed by proper choices of R_3PO probe molecules. For example, zeolites with larger pore sizes such as 12-MR faujasite-type (X or Y) zeolites may be probed by either TMPO, TEPO, or TBPO. As discussed earlier, such ^{31}P - R_3PO NMR approaches are capable of providing important information on acid features, namely, type (Brønsted vs. Lewis), strength, and distribution, and concentration (i.e., relative amounts) of solid acid catalysts simultaneously. Moreover, if applied together with elemental analysis such as ICP-AES/MS, quantitative information (exact acid amounts) of acid sites may also be attained.

As shown in Fig. 2.31A, up to seven resonance peaks at $\delta^{31}P = 86, 75, 67, 63, 53, 43$, and 30 ppm can be identified in the ^{31}P MAS NMR spectrum of TMPO adsorbed on H-ZSM-5 zeolite. The former five downfield signals should be associated with TMPO adsorbed on Brønsted acid sites with varied acid strengths. The signal at 43 ppm was assigned to physisorbed TMPO; this peak remained intact even after the adsorbate-loaded sample was exposed to humidity. The signal at 30 ppm remains unchanged before and after sample silylation treatment, implying that it is likely due to “mobile” TMPO that is either attached in the intercrystalline voids or weakly adsorbed near the channel pore mouths of the zeolite. On the other hand, five characteristic peaks at $\delta^{31}P = 92, 75, 71, 54$, and 47 ppm were observed in the ^{31}P MAS NMR spectrum of TBPO adsorbed on H-ZSM-5 (Fig. 2.31B). The peak at $\delta^{31}P = 47$ ppm was attributed to crystalline TBPO. The resonances at $\delta^{31}P = 92, 75$, and 71 ppm should be related to TBPO adsorbed on the external acid sites, and the signal at 54 ppm was ascribed to physisorbed TBPO. By comparing the $\delta^{31}P$ values of R_3PO ($R = C_nH_{2n+1}$, $n = 1-4$) adsorbed on Brønsted acid sites with the same acidic strength, an average offset of 8 ± 2 ppm was observed based on

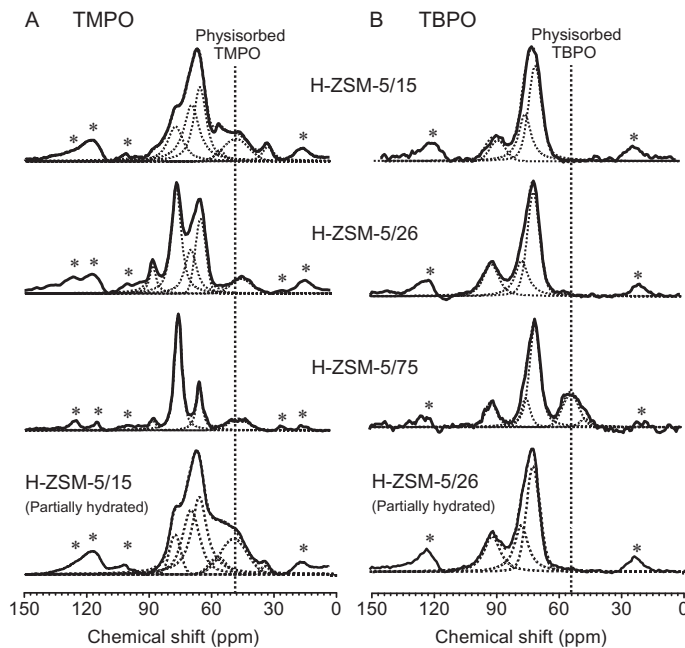


Figure 2.31 ^{31}P MAS NMR spectra of (A) TMPO and (B) TBPO adsorbed on various H-ZSM-5 zeolites with different Si/Al ratios of 15, 26, and 75. The lower spectra were obtained from the H-ZSM-5/15 and H-ZSM/26 samples exposed to humidity for 1.5 h. The dashed curves indicate results of spectral analyses by Gaussian deconvolution. The sample spinning rate is 10 kHz. The asterisks denote spinning sidebands [24].

DFT calculation results for R_3PO with $n \geq 2$ relative to TMPO ($n = 1$) [24]. Accordingly, the results obtained by using the ^{31}P - R_3PO NMR approaches with different probe molecules may be attained to provide information on detailed acid features of solid acid catalysts such as type, concentration, location, and strength of acid sites.

Ryoo and co-workers synthesized MFI zeolites with varied morphology by means of a surfactant as structure-directing agent [76]. The zeolitic catalysts so fabricated were found to exhibit superior catalytic activities during decalin cracking reactions. To correlate the observed reactivity with acid properties of the catalysts, the ^{31}P - R_3PO NMR approaches with TMPO and TBPO probe molecules were exploited. The ^{31}P NMR spectra of TMPO and TBPO adsorbed on various MFI zeolites are compared to a mesoporous Al-MCM-41 aluminosilicate, as shown in Fig. 2.32. The ^{31}P NMR spectrum of TMPO adsorbed on different MFI zeolites exhibited

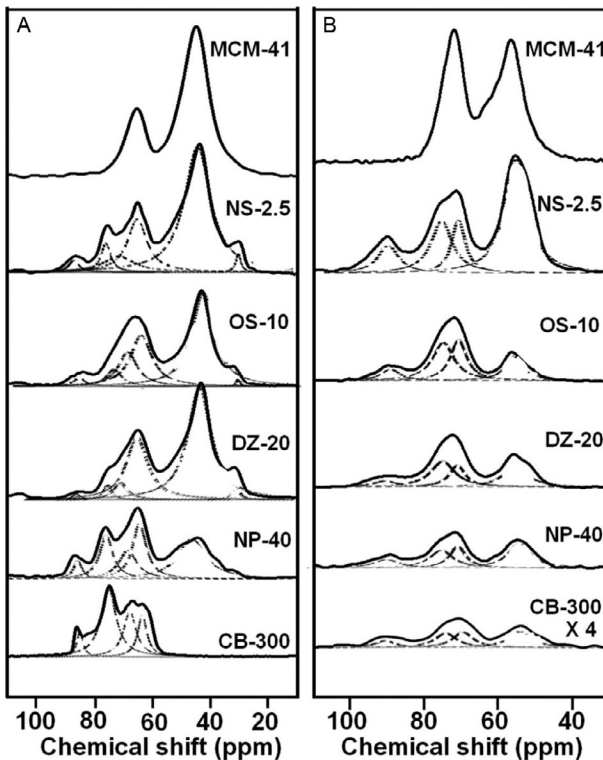


Figure 2.32 ^{31}P MAS NMR spectra of (A) TMPO and (B) TBPO adsorbed on various MFI zeolites. The dashed curves indicate results of spectral analyses by Gaussian deconvolution. All spectra are plotted on the absolute intensity scale after collecting with the same number of acquisitions and being reduced to the same sample mass [76].

up to six resonance peaks with $\delta^{31}\text{P}$ of 30, 42, 66, 68, 76, and 86 ppm (Fig. 2.32A). Among them, the peaks at 30 and 42 ppm were assigned to the mobile and physisorbed TMPO, respectively, whereas the signals at downfield were attributed to TMPO chemisorbed on Brønsted acid sites. In other words, four types of Brønsted acid sites with different acidic strengths, namely, I (86 ppm), II (76 ppm), III (68 ppm), and IV (66 ppm), were present in the MFI samples. Among them, type I sites appear to possess an acidic strength close to the threshold of superacidity ($\delta^{31}\text{P} \geq 86$ ppm) [18]. It is noteworthy that, since the size of TMPO is comparable to the pore aperture of typical 10-MR zeolite, the results obtained from the ^{31}P -TMPO NMR therefore contain information of both internal (intracrystalline) and external (extracrystalline) acid sites of the MFI zeolite samples as in the case of Al-MCM-41.

However, notable differences in the ^{31}P NMR spectra of MFI zeolites were observed when TBPO was used as probe, as shown in Fig. 2.32B. Compared to the spectra obtained by the ^{31}P -TMPO approach in Fig. 2.3A, the major differences of spectra in Fig. 2.32B arose not only from the anticipated intrinsic $\delta^{31}\text{P}$ difference (ca. 8 ± 2 ppm) [25] between the TBPO and the TMPO probe molecules but also due to the fact that the size of TBPO is too bulky to enter the micropores of MFI zeolite; hence, it can only probe acid sites located on external surfaces. In this regard, the three distinct ^{31}P resonances at 92, 74, and 72 ppm were exclusively arising from TBPO adsorbed on extracrystalline Brønsted acidic sites. Accordingly, the three peaks observed from the adsorbed TBPO may be correlated with the peaks obtained from TMPO as followed: 92 ppm (I), 74 ppm (III), and 72 ppm (IV). In this context, it is indicative that type II acid sites are exclusively located in intracrystalline voids of the MFI catalysts regardless of their differences in morphology (mainly crystalline thickness). Further quantitative information such as exact acid amounts corresponding to ^{31}P resonance peaks with different $\delta^{31}\text{P}$ values (i.e. acidic strengths) may be attained if analysed in conjunction with elemental analysis data. In practice, the amount of external acid sites may be obtained from peak areas corresponding to the adsorbed TBPO by first excluding the contribution from physisorbed TBPO. Accordingly, the amount of internal acid sites may be derived by subtracting the external amount obtained earlier from the total peak areas of the adsorbed TMPO (excluding contributions from mobile and physisorbed TMPO). As a result, it was found that the fraction of external acid amount increased with decreasing crystalline thickness of the zeolite. For example, the fraction of external acidity increased from 5% of the conventional CB-300 crystalline bulk zeolite to ca. 32% of the NS-2.5 zeolite nanosheet. Moreover, a linear correlation between the number of strongest external acid sites (i.e. type I from TBPO result) and the catalytic activity of these MFI samples during decalin cracking may be inferred, indicating that the reaction took place exclusively on the external surfaces of the catalysts [76].

Besides trialkylphosphine oxide (R_3PO) molecules, PPh_3 ($11.7 \times 7.1 \text{ \AA}$) [30] has also been applied to probe acid sites in solid acid catalysts. Separate study using molecular mechanical simulations has revealed that the pyramidal shape PPh_3 molecule prefers to adsorb on the 12-MR external surface pockets ($7.1 \times 9.2 \text{ \AA}$) of the MCM-22 zeolite through partial intrusion (see Fig. 2.33) [77] and is hence only capable of probing acid sites in the external surface pockets. The ^{31}P MAS NMR spectrum of PPh_3 adsorbed

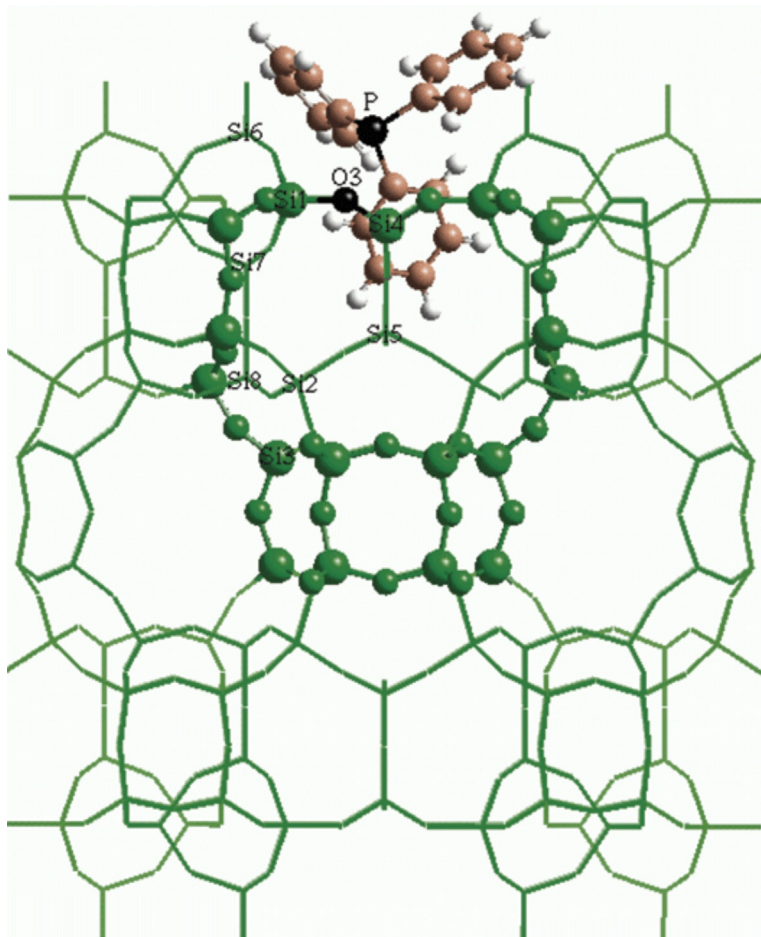


Figure 2.33 Optimized structure of the PPh_3 adsorbed on unit cell of MCM-22 zeolite. The balls in green indicate external surface pocket [77].

on H-MCM-22 zeolites ($\text{SiO}_2/\text{Al}_2\text{O}_3 = 32$) shows three distinct resonances at 14.8, 11.1, and -4.6 ppm (Fig. 2.34). While the latter peak may be assigned due to physisorbed phosphine, the other peaks at downfield should be related to protonated PPh_3 bound to Brønsted acid sites with varied acidic strengths in H-MCM-22 zeolite. Further incorporating the ^{31}P NMR results with elemental analysis data confirmed that ca. 6% of total Brønsted acid sites are located at the pore openings of the external surface pockets [77].

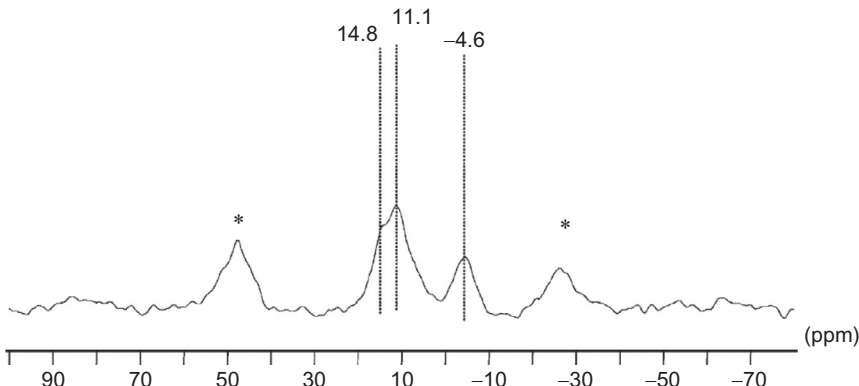


Figure 2.34 ^{31}P MAS NMR spectrum of PPh_3 adsorbed on H-MCM-22 zeolite. The spinning sidebands are indicated by asterisks [77].

In addition to the properties of isolated acid sites, the proximity of acid centres also plays a crucial role during catalytic reactions, particularly for those involving multiple acid sites. In view of the distance (~ 0.30 nm) between the two phosphorus atoms in diphenyldiphosphine ($\text{Ph}_2\text{P}-\text{CH}_2-\text{PPh}_2$), Grey and co-workers used 1D ^{31}P MAS NMR and 2D ^{31}P - ^{31}P DQ NMR of adsorbed diphenyldiphosphines ($\text{Ph}_2\text{P}(\text{CH}_2)_n\text{PPh}_2$; $n=1-6$) to determine the distance between adjacent Brønsted acid sites in solid catalysts [32]. Since the distances between two phosphorus atoms in these diphenyldiphosphines may be tuned by varying the length of the $-\text{CH}_2-$ group, thus, P-P distances of 0.30, 0.56, and 0.94 nm for $\text{Ph}_2\text{P}(\text{CH}_2)_n\text{PPh}_2$ were observed with $n=1$, 3, and 6, respectively. Figure 2.35 showed the ^{31}P MAS NMR spectra of zeolite HY (Si/Al=2.6) loaded with $\text{Ph}_2\text{P}(\text{CH}_2)_n\text{PPh}_2$ ($n=1$, 3, and 6); the resonance at -22 ppm was attributed to weakly physisorbed diphosphine molecules and the peak at -28 ppm to P atoms in more strongly physisorbed phosphine molecules that were either singly protonated or nonprotonated. Since notable $\delta^{31}\text{P}$ enhancements were observed in ^1H - ^{31}P CP MAS experiment, the peaks at -1 , 8, and 14 ppm were assigned to either singly or doubly protonated phosphines.

Additional 2D DQ-SQ (double quantum-single quantum) correlation experiment was also performed to probe the spatial proximity of the two like spins [31]. Typically, dipolar correlation signals arising from spins with identical CSs appear on the diagonal axis of the 2D NMR spectrum, whereas those with different CSs appear as a pair of off-diagonal cross peaks, as illustrated in Fig. 2.22. As such, the CS values of the peaks that appear in the indirect (DQ) dimension should be the sum of CSs of the off-diagonal peak

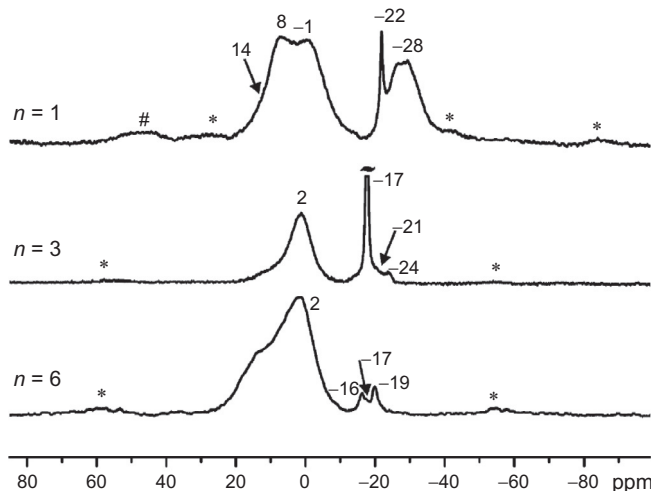


Figure 2.35 ^1H -decoupled ^{31}P MAS NMR spectra of $\text{Ph}_2\text{P}(\text{CH}_2)_n\text{PPh}_2$ adsorbed on a HY zeolite loaded with ca. 12 molecules/unit cell. Spinning speed = 8 kHz. Asterisk denotes spinning sidebands and hash represents overlapping spinning sideband and diphosphine oxide impurity [32].

pair in the direct (SQ) dimension. The cross peaks at (14, -14) and (-28, -14) ppm in Fig. 2.36 reveal that species corresponding to $\delta^{31}\text{P}$ of -28 and 14 ppm are in close proximity. In addition, the diagonal peaks arising from the doubly protonated diphosphine at (8, 16) and (-1, -2) ppm reveal the close proximity of Brønsted acid sites in HY zeolite. Thus, by comparing ^{31}P NMR spectra for different diphenyldiphosphine probe molecules with varying P-P distance (i.e., n value) and loadings, the distance and concentration of acidic sites in zeolites may be determined [32].

3.4. Reaction Mechanism

As mentioned earlier, the ^{31}P SSNMR approaches using various phosphorus-containing probe molecules are capable of providing detailed features of acid sites in solid acid catalysts. By monitoring variations of these acid features (i.e. type, concentration, location, and strength), information on reaction mechanism may also be obtained. For example, TMP has been used as probe to monitor the mechanism of the titanium-substituted silicalite-1 (TS-1) during oxidation reaction. It is well known that TS-1 zeolites are highly active solid acid catalysts for a variety of important oxidation reactions, such as phenol hydroxylation, cyclohexanone ammoximation, and propylene oxidation [58]. However, the distribution

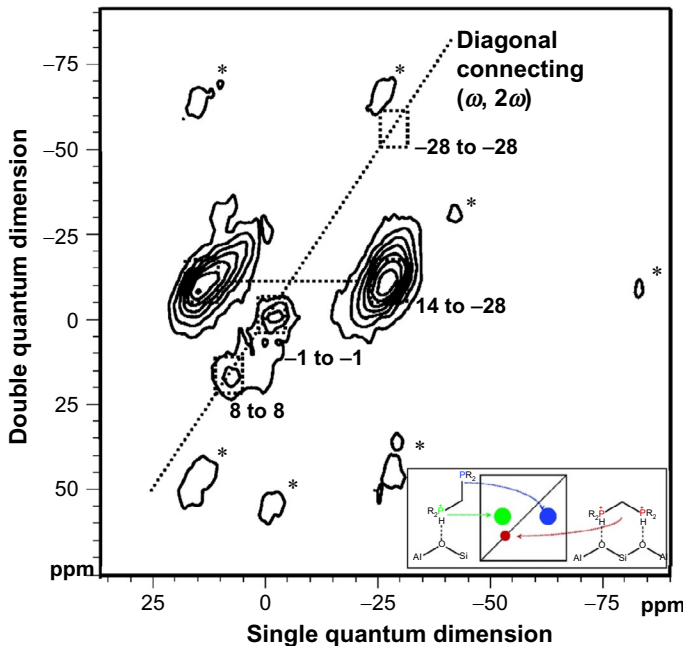


Figure 2.36 2D ^{31}P DQ NMR spectra of $\text{Ph}_2\text{P}(\text{CH}_2)\text{PPh}_2$ (loading ca. 8 molecules/unit cell). Following ^1H - ^{31}P CP, a post-C7 DQ sequence was adopted to prepare and then to reconvert DQ coherences using a DQ excitation time of 2 ms and MAS spinning speed of 8 kHz. Asterisk denotes spinning sidebands [32].

of Ti in the structural framework and consequently the active site responsible for the high catalytic activity observed for TS-1 during oxidation reactions remain largely unknown. By adopting the ^{31}P -TMP NMR approach *in situ*, Zhuang *et al.* demonstrated that the various Ti sites in TS-1 zeolite, which serve as active centres during oxidation reaction, may be identified, as shown in Fig. 2.37 [78]. For TS-1 before the oxidation treatment (in air), the corresponding ^{31}P NMR spectrum of the adsorbed TMP that reveals as many as five resonance peaks was explicitly observed (Fig. 2.37A). The peak at -4.8 ppm was assigned to $[(\text{CH}_3)_3\text{PH}]^+$ ion protonated by mainly TiOH (and partly by SiOH) of the framework $\text{Ti}(\text{OSi})_3\text{OH}$ species [79]. The signals at -62.1 and -59.8 ppm may be attributed to the physisorbed TMP, whereas the peaks at -34.2 and -32.0 ppm were ascribed due to TMP adsorbed on Lewis acid sites with different acidic strengths [80,81]. Further investigation by theoretical calculations confirmed that the presences of $\text{Ti}(\text{OSiO}_3)_4$ and

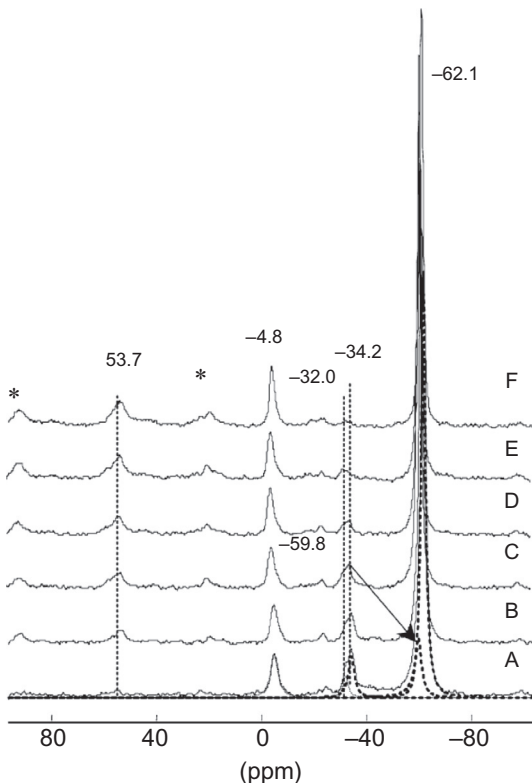


Figure 2.37 Variations of ^{31}P MAS NMR spectra of TMP adsorbed on TS-1 zeolite (A) before and after oxidation treatment at 343 K in air for different exposure periods of time: (B) 10 min, (C) 20 min, (D) 30 min, (E) 40 min, and (F) 50 min. The asterisks denote spinning sidebands [78].

$(\text{OSiO}_3)_3\text{Ti(OH)}$ species are most likely the origins of Lewis acid sites that are responsible for the peaks with $\delta^{31}\text{P}$ at -34.2 and -32.0 ppm, respectively [80,81].

Immediately after the catalyst was exposed to oxygen, notable decrease in the intensity of the ^{31}P resonance at -34.2 ppm accompanied by the appearance of a new resonance peak at 53.7 ppm was evident (Fig. 2.37B). The authors assigned the latter downfield peak to TMPO bound to Lewis acid sites [78]. It was estimated that after exposing the TS-1 catalyst in air for 10 min, ca. 46% of the peak area of the resonance at -34.2 ppm (for TMP adsorbed on Lewis acid sites) was converted to the Lewis-bound TMPO (at 53.7 ppm), while no significant changes in intensities of other ^{31}P resonances were observed. Moreover, a progressive increase in peak

intensity of the signal at 53.7 ppm at the expanse of the resonance at -34.2 ppm with increasing exposure time was observed. The peak responsible for TMP bound to Lewis acid sites with weaker acidic strength eventually diminished at an extended exposure time of about 40 min (Fig. 2.37E). It is noted that as the exposure time exceeded ca. 30 min, the peak intensity of the resonance at -32.0 ppm also begins to decrease, indicating the subsequent oxidation of the TMP species bound to the stronger Lewis acid sites. Almost all of the Lewis-bound TMP species were oxidized to form TMPO after exposure in air for 50 min. In contrast, the resonance that corresponds to protonated TMPh^+ ion remained practically intact in the presence of oxidation treatment, suggesting the inability of $\text{Ti(OSi)}_3\text{OH}$ species in TS-1 to catalyse the oxidation of TMP under such experimental conditions. Thus, it is indicative that Lewis acid sites (i.e., unsaturated tricoordinated Ti) in TS-1 serve as the primary oxidation centres for TMP conversion. Accordingly, the results obtained from this *in situ* ^{31}P -TMP NMR approach readily provide information on mechanism and activity of TS-1 during oxidation reaction [78].



4. SUMMARY

We have demonstrated that the ^{31}P SSNMR of adsorbed phosphorus-containing probe molecules (viz., TMP, R_3PO , phosphines, and diphosphines) represents a unique and practical technique for comprehensive acidity characterization of solid acid catalysts. Detailed acid features, namely, type, distribution, accessibility (location/proximity), concentration (amount), and strength of acid sites in solid acids, may readily be obtained both qualitatively and quantitatively. By comparison, the ^{31}P -TMP NMR approach is found to be viable for discerning acid types in the solid acids and more sensitive for probing Lewis acidity, whereas the ^{31}P -TMPO NMR approach is more useful for determining the Brønsted acid strength of solid acids and capable of covering the whole range from weak, medium, strong, all the way to superacidity. Moreover, by properly choosing trialkylphosphine oxide probe molecules with different sizes (viz., TMPO, TEPO, TBPO, and TOPO), the ^{31}P - R_3PO NMR approaches may be applied to distinguish acid sites located in internal or external surfaces of porous solid acid catalysts. In addition, the proximity and distance between adjacent Brønsted acid sites can be estimated by 2D ^{31}P - ^{31}P DQ NMR technique by using diphenyldiphosphines ($\text{Ph}_2\text{P}(\text{CH}_2)_n\text{PPh}_2$; $n=1-6$) as the probes. These ^{31}P SSNMR approaches for acidity characterization invoking

various phosphorus-containing probe molecules, if properly exploited with *in situ* and/or *ex situ* experimental techniques, are most practical not only for probing the variations of acid features in solid acids but also for understanding synergy effect among multiple acid sites and possible reaction mechanism (activity and selectivity) in heterogeneous catalysis.

ACKNOWLEDGEMENTS

This work was supported by the National Natural Science Foundation of China (21173255, 21073228, 20933009, and 21210005) and the National Science Council of Taiwan (NSC-101-2113-M-001-020-MY3). AMZ is grateful for the visiting research fellowship from the Department of Chemistry and Catalysis Research Center, Technische Universität München.

REFERENCES

- [1] G. Busca, Acid catalysts in industrial hydrocarbon chemistry, *Chem. Rev.* 107 (2007) 5366–5410.
- [2] A. Zecchina, S. Bordiga, C. Lamberti, G. Spoto, L. Carnelli, Areán C. Otero, Low-temperature Fourier transform infrared study of the interaction of CO with cations in alkali-metal exchanged ZSM-5 zeolites, *J. Phys. Chem.* 98 (1994) 9577–9582.
- [3] P. Sarv, T. Tuherm, E. Lippmaa, E. Keskinen, A. Root, Mobility of the acidic proton in Broensted sites of H-Y, H-mordenite, and H-ZSM-5 zeolites, studied by high-temperature ^1H MAS NMR, *J. Phys. Chem.* 99 (1995) 13763–13768.
- [4] H.M. Kao, C.P. Grey, Probing the Brønsted and Lewis acidity of zeolite HY: a $^1\text{H}/^{27}\text{Al}$ and $^{15}\text{N}/^{27}\text{Al}$ TRAPDOR NMR study of monomethylamine adsorbed on HY, *J. Phys. Chem.* 100 (1996) 5105–5117.
- [5] W.E. Farneth, R.J. Gorte, Methods for characterizing zeolite acidity, *Chem. Rev.* 95 (1995) 615–636.
- [6] D. Freude, M. Hunger, H. Pfeifer, W. Schwieger, ^1H MAS NMR studies on the acidity of zeolites, *Chem. Phys. Lett.* 128 (1986) 62–66.
- [7] L. Liu, L. Zhao, H. Sun, Simulation of NH_3 temperature-programmed desorption curves using an *ab initio* force field, *J. Phys. Chem. C* 113 (2009) 16051–16057.
- [8] H. Pfeifer, H. Ernst, NMR studies of zeolites, *Annu. Rep. NMR Spectrosc.* 28 (1994) 91–187.
- [9] M. Hunger, Brønsted acid sites in zeolites characterized by multinuclear solid-state NMR spectroscopy, *Catal. Rev. Sci. Eng.* 39 (1997) 345–393.
- [10] M. Xu, A. Arnold, A. Buchholz, W. Wang, M. Hunger, Low-temperature modification of mesoporous MCM-41 material with sublimated aluminum chloride in vacuum, *J. Phys. Chem. B* 106 (2002) 12140–12143.
- [11] J.F. Haw, J.B. Nicholas, T. Xu, L.W. Beck, D.B. Ferguson, Physical organic chemistry of solid acids: lessons from *in situ* NMR and theoretical chemistry, *Acc. Chem. Res.* 29 (1996) 259–267.
- [12] D.H. Barich, J.B. Nicholas, T. Xu, J.F. Haw, Theoretical and experimental study of the ^{13}C chemical shift tensors of acetone complexed with Brønsted and Lewis acids, *J. Am. Chem. Soc.* 120 (1998) 12342–12350.
- [13] J.H. Lunsford, W.P. Rothwell, W. Shen, Acid sites in zeolite Y: a solid-state NMR and infrared study using trimethylphosphine as a probe molecule, *J. Am. Chem. Soc.* 107 (1985) 1540–1547.

- [14] H.M. Kao, C.P. Grey, Characterization of the Lewis acid sites in zeolite HY with the probe molecule trimethylphosphine, and $^{31}\text{P}/^{27}\text{Al}$ double resonance NMR, *Chem. Phys. Lett.* 259 (1996) 459–464.
- [15] Y. Chu, Z. Yu, A. Zheng, H. Fang, H. Zhang, S.J. Huang, S.B. Liu, F. Deng, Acidic strengths of Brønsted and Lewis acid sites in solid acids scaled by ^{31}P NMR chemical shifts of adsorbed trimethylphosphine, *J. Phys. Chem. C* 115 (2011) 7660–7667.
- [16] Y. Wang, F. Wang, Q. Song, Q. Xin, S. Xu, J. Xu, Heterogeneous ceria catalyst with water-tolerant Lewis acidic sites for One-Pot synthesis of 1,3-diols via prins condensation and hydrolysis reactions, *J. Am. Chem. Soc.* 135 (2013) 1506–1515.
- [17] A. Zheng, S.B. Liu, F. Deng, Acidity characterization of heterogeneous catalysts by solid-state NMR spectroscopy using probe molecules, *Solid State Nucl. Magn. Reson.* (2013) 55–56, 12–27.
- [18] A. Zheng, H. Zhang, X. Lu, S.B. Liu, F. Deng, Theoretical predictions of ^{31}P NMR chemical shift threshold of trimethylphosphine oxide absorbed on solid acid catalysts, *J. Phys. Chem. B* 112 (2008) 4496–4505.
- [19] J. Xu, A. Zheng, J. Yang, Y. Su, J. Wang, D. Zeng, M. Zhang, C. Ye, F. Deng, Acidity of mesoporous $\text{MoO}_x/\text{ZrO}_2$ and WO_x/ZrO_2 materials: a combined solid-state NMR and theoretical calculation study, *J. Phys. Chem. B* 110 (2006) 10662–10671.
- [20] T. Riemer, H. Knözinger, ^{31}P Solid state NMR and ESR investigation of trimethylphosphane adsorption on zirconia and sulfated zirconia, *J. Phys. Chem.* 100 (1996) 6739–6742.
- [21] J. Yang, M.J. Zhang, F. Deng, Q. Luo, D.Y. Yi, C.H. Ye, Solid state NMR study of acid sites formed by adsorption of SO_3 onto $\gamma\text{-Al}_2\text{O}_3$, *Chem. Commun.* 7 (2003) 884–885.
- [22] H. Zhang, H. Yu, A. Zheng, S. Li, W. Shen, F. Deng, Reactivity enhancement of 2-propanol photocatalysis on $\text{SO}_4^{2-}/\text{TiO}_2$: insights from solid-state NMR spectroscopy, *Environ. Sci. Technol.* 42 (2008) 5316–5321.
- [23] G.E. Maciel, P.D. Ellis, NMR characterization of silica and alumina surfaces, in: A.T. Bell, A. Pines (Eds.), *NMR Techniques in Catalysis*, vol. 55, Marcel Dekker, New York, 1994, p. 231.
- [24] Q. Zhao, W.H. Chen, S.J. Huang, Y.C. Wu, H.K. Lee, S.B. Liu, Discernment and quantification of internal and external acid sites on zeolites, *J. Phys. Chem. B* 106 (2002) 4462–4469.
- [25] A. Zheng, S.J. Huang, W.H. Chen, P.H. Wu, H. Zhang, H.K. Lee, L.C. De Ménorval, F. Deng, S.B. Liu, ^{31}P Chemical shift of adsorbed trialkylphosphine oxides for acidity characterization of solid acids catalysts, *J. Phys. Chem. A* 112 (2008) 7349–7356.
- [26] W.H. Chen, H.H. Ko, A. Sakthivel, S.J. Huang, S.H. Liu, A.Y. Lo, T.C. Tsai, S.B. Liu, A solid-state NMR, FT-IR and TPD study on acid properties of sulfated and metal-promoted zirconia: influence of promoter and sulfation treatment, *Catal. Today* 116 (2006) 111–120.
- [27] H.H. Ko, Preparation, modification, and characterization of metal-oxide and nanosized aluminosilicate solid acid catalysts, MS thesis, Department of Materials Science and Nanotechnology, Chinese Culture University, Taipei, Taiwan, June 2005.
- [28] A. Zheng, S.J. Huang, S.B. Liu, F. Deng, Acid properties of solid acid catalysts characterized by solid-state ^{31}P NMR of adsorbed phosphorous probe molecules, *Phys. Chem. Chem. Phys.* 13 (2011) 14889–14901.
- [29] Q. Zhao, W.H. Chen, S.J. Huang, S.B. Liu, Qualitative and quantitative determination of acid sites on solid acid catalysts, *Stud. Surf. Sci. Catal.* 145 (2003) 205–209.
- [30] C.S. Hsia Chen, S.E. Schramm, Type and catalytic activity of surface acid sites of medium and large pore zeolites: their deactivation with bulky organophosphorus compounds, *Microporous Mater.* 7 (1996) 125–132.

- [31] M. Hohwy, H.J. Jakobsen, M. Eden, M.H. Levitt, N.C. Nielsen, Broadband dipolar recoupling in the nuclear magnetic resonance of rotating solids: a compensated C7 pulse sequence, *J. Chem. Phys.* 108 (1998) 2686–2694.
- [32] L. Peng, P.J. Chupas, C.P. Grey, Measuring Brønsted acid densities in zeolite HY with diphosphine molecules and solid state NMR spectroscopy, *J. Am. Chem. Soc.* 126 (2004) 12254–12255.
- [33] L.M. Kustov, V.B. Kazansky, F. Figueras, D. Tichit, Investigation of the acidic properties of ZrO_2 Modified by SO_4^{2-} anions, *J. Catal.* 150 (1994) 143–149.
- [34] F. Babou, G. Coudurier, J.C. Vedrine, Acidic properties of sulfated zirconia: an infrared spectroscopic study, *J. Catal.* 152 (1995) 341–349.
- [35] A. Corma, V. Fornés, M.I. Juan-Rajadell, J.M. López Nieto, Influence of preparation conditions on the structure and catalytic properties of $\text{SO}_4^{2-}/\text{ZrO}_2$ superacid catalysts, *Appl. Catal. A* 116 (1994) 151–163.
- [36] S.J. Huang, Y.H. Tseng, Y. Mou, S.B. Liu, S.H. Huang, C.P. Lin, J.C.C. Chan, Spectral editing based on selective excitation and Lee-Goldburg cross-polarization under magic angle spinning, *Solid State Nucl. Magn. Reson.* 29 (2006) 272–277.
- [37] B.J. Van Rossum, C.P. De Groot, V. Ladizhansky, S. Vega, H.J.M. De Groot, A method for measuring heteronuclear ($^1\text{H} - ^{13}\text{C}$) distances in high speed MAS NMR, *J. Am. Chem. Soc.* 122 (2000) 3465–3472.
- [38] V. Ladizhansky, S. Vega, Polarization transfer dynamics in Lee-Goldburg cross polarization nuclear magnetic resonance experiments on rotating solids, *J. Chem. Phys.* 112 (2000) 7158–7168.
- [39] C.P. Grey, W.S. Veeman, A.J. Vega, Rotational echo $^{14}\text{N}/^{13}\text{C}/^1\text{H}$ triple resonance solid-state nuclear magnetic resonance: a probe of $^{13}\text{C} - ^{14}\text{N}$ internuclear distances, *J. Chem. Phys.* 98 (1993) 7711–7725.
- [40] M.D. Karra, K.J. Stutovich, K.T. Mueller, NMR characterization of Brønsted acid sites in faujasitic zeolites with Use of perdeuterated trimethylphosphine oxide, *J. Am. Chem. Soc.* 124 (2002) 902–903.
- [41] B. Alonso, I. Klur, D. Massiot, Studies of surfaces through molecular probe adsorption and solid-state NMR, *Chem. Commun.* 8 (2002) 804–805.
- [42] L. Baltusis, J.S. Frye, G.E. Maciel, Phosphine oxides as NMR probes for adsorption sites on surfaces, *J. Am. Chem. Soc.* 108 (1986) 7119–7120.
- [43] H.M. Kao, C.Y. Yu, M.C. Yeh, Detection of the inhomogeneity of Brønsted acidity in H-mordenite and H- β zeolites: a comparative NMR study using trimethylphosphine and trimethylphosphine oxide as ^{31}P NMR probes, *Microporous Mesoporous Mater.* 53 (2002) 1–12.
- [44] Catalysis Commission, International Zeolite Association. <http://www.iza-online.org/catalysis/>.
- [45] B.M. Weckhuysen, D. Wang, M.P. Rosynek, J.H. Lunsford, Conversion of methane to benzene over transition metal ion ZSM-5 zeolites: I. catalytic characterization, *J. Catal.* 175 (1998) 338–346.
- [46] Y. Xu, L. Lin, Recent advances in methane dehydro-aromatization over transition metal ion-modified zeolite catalysts under non-oxidative conditions, *Appl. Catal. A* 188 (1999) 53–67.
- [47] Y. Shu, D. Ma, L. Xu, Y. Xu, X. Bao, Methane dehydro-aromatization over Mo/MCM-22 catalysts: a highly selective catalyst for the formation of benzene, *Catal. Lett.* 70 (2000) 67–73.
- [48] S.J. Huang, Q. Zhao, W.H. Chen, X. Han, X. Bao, P.S. Lo, H.K. Lee, S.B. Liu, Structure and acidity of Mo/H-MCM-22 catalysts studied by NMR spectroscopy, *Catal. Today* 97 (2004) 25–34.
- [49] E.L. Tae, K.E. Lee, J.S. Jeong, K.B. Yoon, Synthesis of diamond-shape titanate molecular sheets with different sizes and realization of quantum confinement effect during dimensionality reduction from two to zero, *J. Am. Chem. Soc.* 130 (2008) 6534–6543.

- [50] D.V. Bavykin, F.C. Walsh, Elongated titanate nanostructures and their applications, *Eur. J. Inorg. Chem.* 8 (2009) 977–997.
- [51] M. Kitano, E. Wada, K. Nakajima, S. Hayashi, S. Miyazaki, H. Kobayashi, M. Hara, Protonated titanate nanotubes with Lewis and Brønsted acidity: relationshipt between nanotube structure and catalytic activity, *Chem. Mater.* 25 (2013) 385–393.
- [52] E.F. Rakiewicz, A.W. Peters, R.F. Wormsbecher, K.J. Sutovich, K.T. Mueller, Characterization of acid sites in zeolitic and other inorganic systems using solid-state ^{31}P NMR of the probe molecule trimethylphosphine oxide, *J. Phys. Chem. B* 102 (1998) 2890–2896.
- [53] C. Tagusagawa, A. Takagaki, S. Hayashi, K. Domen, Evaluation of strong acid properties of layered HNbMoO_6 and catalytic activity for Friedel-Crafts alkylation, *Catal. Today* 142 (2009) 267–271.
- [54] A. Takagaki, C. Tagusagawa, S. Hayashi, M. Hara, K. Domen, Nanosheets as highly active solid acid catalysts for green chemical syntheses, *Energy Environ. Sci.* 3 (2010) 82–93.
- [55] C. Tagusagawa, A. Takagaki, S. Hayashi, K. Domen, Characterization of HNbWO_6 and HTaWO_6 metal oxide nanosheet aggregates as solid acid catalysts, *J. Phys. Chem. C* 113 (2009) 7831–7837.
- [56] C. Tagusagawa, A. Takagaki, A. Iguchi, K. Takanabe, J.N. Kondo, K. Ebitani, S. Hayashi, T. Tatsumi, K. Domen, Highly active mesoporous Nb-W oxide solid-acid catalyst, *Angew. Chem. Int. Ed. Engl.* 49 (2010) 1128–1132.
- [57] J. Fierro, *Metal Oxides: Chemistry and Applications*, CRC Press, Boca Raton, FL, 2006.
- [58] C. Perego, A. Carati, P. Ingallina, M.A. Mantegazza, G. Bellussi, Production of titanium containing molecular sieves and their application in catalysis, *Appl. Catal. A* 221 (2001) 63–72.
- [59] S. Li, H. Zhou, B. Han, F. Deng, X. Liu, L. Xiao, J. Fan, Hydrogenated mesoporous $\text{TiO}_2\text{--SiO}_2$ with increased moderate strong Brønsted acidic sites for Friedel-Crafts alkylation reaction, *Catal. Sci. Technol.* 2 (2012) 719–721.
- [60] A. Corma, Inorganic solid acids and their Use in acid-catalyzed hydrocarbon reactions, *Chem. Rev.* 95 (1995) 559–614.
- [61] J.A. Moreno, G. Poncet, Isomerization of *n*-butane over sulfated Al- and Ga-promoted zirconium oxide catalysts. Influence of promoter and preparation method, *J. Catal.* 203 (2001) 453–465.
- [62] K. Föttinger, K. Zorn, H. Vinek, Influence of the sulfate content on the activity of Pt containing sulfated zirconia, *Appl. Catal. A* 284 (2005) 69–75.
- [63] N. Feng, A. Zheng, S.J. Huang, H. Zhang, N. Yu, C.Y. Yang, S.B. Liu, F. Deng, Combined solid-state NMR and theoretical calculation studies of Brønsted acid properties in anhydrous 12-molybdophosphoric acid, *J. Phys. Chem. C* 114 (2010) 15464–15472.
- [64] T. Okuhara, H. Watanabe, T. Nishimura, K. Inumaru, M. Misono, Microstructure of cesium hydrogen salts of 12-tungstophosphoric acid relevant to novel acid catalysis, *Chem. Mater.* 12 (2000) 2230–2238.
- [65] U. Filek, A. Bressel, B. Sulikowski, M. Hunger, Structural stability and Brønsted acidity of thermally treated $\text{AlPW}_{12}\text{O}_{40}$ in comparison with $\text{H}_3\text{PW}_{12}\text{O}_{40}$, *J. Phys. Chem. C* 112 (2008) 19470–19476.
- [66] S.J. Huang, C.Y. Yang, A. Zheng, N. Feng, N. Yu, P.H. Wu, Y.C. Chang, Y.C. Lin, F. Deng, S.B. Liu, New insights into Keggin-type 12-tungstophosphoric acid from ^{31}P MAS NMR analysis of absorbed trimethylphosphine oxide and DFT calculations, *Chem. Asian J.* 6 (2011) 137–148.
- [67] F. De Clippele, M. Dusselier, R. Van Rompaey, P. Vanelderen, J. Dijkmans, E. Makshina, L. Giebel, S. Oswald, G.V. Baron, J.F. Denayer, P.P. Pescarmona,

- P.A. Jacobs, B.F. Sels, Fast and selective sugar conversion to alkyl lactate and lactic acid with bifunctional carbon–silica catalysts, *J. Am. Chem. Soc.* 134 (2012) 10089–10101.
- [68] F. Liu, A. Zheng, I. Noshadi, F.S. Xiao, Design and synthesis of hydrophobic and stable mesoporous polymeric solid acid with ultra strong acid strength and excellent catalytic activities for biomass transformation, *Appl. Catal. B* 136–137 (2013) 193–201.
- [69] S. Suganuma, K. Nakajima, M. Kitano, H. Kato, A. Tamura, H. Kondo, S. Yanagawa, S. Hayashi, M. Hara, SO₃H-bearing mesoporous carbon with highly selective catalysis, *Microporous Mesoporous Mater.* 143 (2011) 443–450.
- [70] D. Zeng, S. Liu, W. Gong, G. Wang, J. Qiu, Y. Tian, Acid properties of solid acid from petroleum coke by chemical activation and sulfonation, *Catal. Commun.* 40 (2013) 5–8.
- [71] Y.Y. Li, S.P. Perera, B.D. Crittenden, J. Bridgwater, The effect of the binder on the manufacture of a 5A zeolite monolith, *Powder Technol.* 116 (2001) 85–96.
- [72] M. Raimondo, G. Perez, A. De Stefanis, A.A.G. Tomlinson, O. Ursini, PLS vs. Zeolites as sorbents and catalysts 4. Effects of acidity and porosity on alkylation of benzene by primary alcohols, *Appl. Catal. A* 164 (1997) 119–126.
- [73] L.D. Rollmann, D.E. Walsh, Shape selectivity and carbon formation in zeolites, *J. Catal.* 56 (1979) 139–140.
- [74] A.R. Pradhan, J.F. Wu, S.J. Jong, W.H. Chen, T.C. Tsai, S.B. Liu, Influences of zeolite structure on formation and location of coke: A¹²⁹Xe and ¹³C CP-MAS NMR study, *Appl. Catal. A* 159 (1997) 187–209.
- [75] W.H. Chen, S.J. Huang, C.S. Lai, T.C. Tsai, H.K. Lee, S.B. Liu, Effects of binder, coking and regeneration on acid properties of H-mordenite during TDP reaction, *Res. Chem. Intermed.* 29 (2003) 761–772.
- [76] Y. Seo, K. Cho, Y. Jung, R. Ryoo, Characterization of the surface acidity of MFI zeolite nanosheets by ³¹P NMR of adsorbed phosphine oxides and catalytic cracking of decalin, *ACS Catal.* 3 (2013) 713–720.
- [77] Y. Wang, J. Zhuang, G. Yang, D. Zhou, D. Ma, X. Han, X. Bao, Study on the external surface acidity of MCM-22 zeolite: theoretical calculation and ³¹P MAS NMR, *J. Phys. Chem. B* 108 (2004) 1386–1391.
- [78] J. Zhuang, D. Ma, Z. Yan, F. Deng, X. Liu, X. Han, X. Bao, X. Liu, X. Guo, X. Wang, Solid-State MAS NMR detection of the oxidation center in TS-1 zeolite by *in situ* probe reaction, *J. Catal.* 221 (2004) 670–673.
- [79] J. Zhuang, Z. Yan, X. Liu, X. Liu, X. Han, X. Bao, U. Müller, NMR study on the acidity of TS-1 zeolite, *Catal. Lett.* 83 (2002) 87–91.
- [80] G. Yang, J. Zhuang, D. Ma, X. Lan, L. Zhou, X. Liu, X. Han, X. Bao, A joint experimental-theoretical study on trimethylphosphine adsorption on the Lewis acidic sites present in TS-1 zeolite, *J. Mol. Struct.* 882 (2008) 24–29.
- [81] G. Yang, X. Lan, J. Zhuang, D. Ma, L. Zhou, X. Liu, X. Han, X. Bao, Acidity and defect sites in titanium silicalite catalyst, *Appl. Catal. A* 337 (2008) 58–65.